
This manuscript is a preprint and has not undergone peer-review. Subsequent versions of this manuscript may have different content. If accepted, the final version of this manuscript will be available via the '*Peer-reviewed Publication DOI*' link on the right-hand side of this webpage. Please feel free to contact any of the authors directly or to comment on the manuscript using **hypothes.is** (<https://web.hypothes.is/>). We welcome feedback!

1 The role of mass-transport complexes (MTCs) in the initiation and
2 evolution of submarine canyons

3 Nan Wu^{1*}, Harya D. Nugraha², Guangfa Zhong¹, Michael J. Steventon³

4 ¹State Key Laboratory of Marine Geology, Tongji University, Shanghai 200092, China

5 ²Center for Sustainable Geoscience, Universitas Pertamina, Jakarta, 12220, Indonesia

6 ³Shell Research, Shell Centre, London, SE1 7NA, UK.

7 *Email: nanwu@tongji.edu.cn

8 **Abstract**

9 The offshore area of the Otway Basin (SE Australia) is dominated by a multibranched canyon system
10 where mass-transport complexes (MTCs) are widely distributed. Our study integrates high-
11 resolution multi-beam and seismic data to investigate the importance of MTCs in dictating the
12 evolution of canyons. Our study interprets three regionally distributed MTCs that fail
13 retrogressively and affect almost 70% of the study area. Within the MTCs, seven canyons that
14 initiated from the continental shelf edge and extended to the abyssal plain are observed. Although
15 the canyons share common regional tectonics and oceanography, the scales, morphology, and
16 distribution are distinctly different. This is linked to the presence of failure-related scarps that
17 control the initiation and formation of the canyons. The retrogressive failure mechanisms of MTCs
18 have created a series of scarps on the continental shelf and slope regions. In the continental shelf,
19 where terrestrial input is absent, the origin of the canyons is related to the local failures and
20 contour current activities, occurring near the pre-existing larger headwall scarps (c. 120 m high,
21 3km long). The occurrence of these local failures has provided the necessary sediment input for
22 subsequent gravity-driven, downslope sediment flows. In the continental slope region, the
23 widespread scarps can capture gravity flows initiated from the continental shelf, developing an
24 area of flow convergence, which greatly widens and deepens the canyon system. The gradual
25 diversion and convergence through MTC related scarps have facilitated the canyon confluence
26 process, which has fundamentally changed the canyoning process. Thus, this study concludes that

27 the retrogressive failure mechanism of MTCs has a direct contribution to the initiation, distribution,
28 and evolution of the canyons. The scarps associated with MTCs have greatly facilitated the delivery
29 of sediments and marine plastics from the shelf edge into the deep oceans, especially in areas
30 where fluvial input is missing.

31 Keywords: Mass-transport complexes (MTCs); Submarine canyons; Otway Basin; SE Australia

32 1. Introduction

33 Submarine canyons are defined as steep-sided V- or U-shaped valleys that erode into the seabed,
34 they can extend from the continental shelf to the continental slope, with numerous tributaries
35 entering from both sides (Shepard et al., 1966; Twichell and Roberts, 1982; Obelcz et al., 2014).
36 Canyons are complex geomorphological features formed by erosion from gravity flows occurring
37 near subaqueous slopes (Shepard, 1972; Canals et al., 2006; Harris and Whiteway, 2011). Canyons
38 are often associated with sand-rich gravity flows and submarine fans are thus considered as
39 modern analogues for deepwater hydrocarbon reservoirs (Stow and Mayall, 2000; Weimer and
40 Slatt, 2004). Mass-transport complexes (MTCs) are gravity-driven shear failure deposits resulting
41 from creep, spread, slide, slump and debris flow processes (Posamentier and Martinsen, 2011; Wu
42 et al., 2021). MTCs can be extremely erosive, thus containing large volumes of sediments, with
43 single deposits covering areas of $>100 \text{ km}^2$ and volumes of $>10,000 \text{ km}^3$ (Frey Martinez et al., 2005;
44 Moscardelli and Wood, 2016; Nugraha et al., 2019). MTCs normally fail retrogressively (i.e.
45 backstepping slope failures), the emplacement of MTCs can leave a series of giant slide scars (c.2-
46 5 km wide) on continental slope areas (Figure 1a, 1b; i.e. Williams, 2016; Li et al., 2017). Both MTCs
47 and canyons can transfer large amounts of sediments between the continental shelf and abyssal
48 plain environments, and are considered important sediment transportation processes in
49 deepwater settings (McAdoo et al., 2000; Popescu et al., 2004; Antobreh and Krastel, 2006; Lee et
50 al., 2007; Urgeles and Camerlenghi, 2013).

51 Submarine canyons and MTCs can have a close relationship in terms of their spatial distribution,
52 triggering mechanisms, and preconditioning factors (Micallef et al., 2012; Watson et al., 2020). The
53 emplacement of MTCs can represent the early phase of submarine canyon initiation, providing
54 early depressions on the continental slopes that extend to the shelf break (Farre et al., 1983). The

55 continuous downcutting process associated with canyon development can steepen the gradient of
56 canyon sidewalls, which preconditions the the sidewalls to fail depositing MTCs near the canyon
57 walls (i.e. Farre et al., 1983; Green and Uken, 2008). These intra-canyon MTCs can occur
58 retrogressively, increasing the canyon's width (i.e. lateral extension; Pratson and Ryan, 1994) and
59 extending the canyon upslope (i.e. headward incision; Farre et al., 1983; He et al., 2014). Most of
60 the published works have focused on constraining local, coeval, intra-canyon MTCs (sensu
61 detached MTCs; Moscardelli and Wood, 2008) with the evolution of canyons (i.e. Green and Uken,
62 2008; Gong et al., 2011; He et al., 2014; Su et al., 2020). The relationship between canyons with
63 regional distributed MTCs (i.e. 100s to 100,000s of km²) (sensu attached MTCs; Moscardelli and
64 Wood, 2008) that typically fails retrogressively, have largely been overlooked. Relatively little is
65 known on how regionally distributed MTCs, especially how their retrogressive failure mechanism
66 can influence the initiation, evolution, and morphology of submarine canyons. Therefore, this
67 study uses a high-resolution (c. 10 m vertical resolution) 3D seismic reflection dataset, integrated
68 with 2D seismic and multi-beam data to analyse the spatial and temporal relations between
69 canyons and regionally distributed MTCs in the Otway Basin, south-eastern Australia (Figure 2a,
70 2b).

71 2. Geological setting

72 2.1 Tectonic

73 The offshore Otway Basin is a broadly NW-SE striking non-volcanic rift basin, located along the
74 south-eastern Australian passive margin (Figure 2b). The basin was initiated by late Jurassic to early
75 Palaeogene rifting, during the progressive breakup of southern and eastern Gondwana. After
76 experiencing multistage rifting, thermal subsidence and inversion, the south Australian margin
77 ultimately broke-up with Antarctica at the end of the Cretaceous (approximately 67 Ma; Willcox
78 and Stagg, 1990; Perincek and Cockshell, 1995; Krassay et al., 2004; Totterdell et al., 2014).
79 Although the detailed history of the separation and final breakup between Australia and Antarctica
80 remains partially studied (Gibson et al., 2013; Holford et al., 2014), the formation of a regionally
81 distributed Maastrichtian unconformity has been attributed to the eventual separation of the
82 Australian and Antarctica Plates (Figure 3a; Krassay et al., 2004; Holford et al., 2014).

83 2.2 Sedimentology

84 The Cenozoic sedimentary successions in the Otway Basin is composed of marine-related, often
85 calcareous-rich sediments, reflecting an open marine depositional environment (McGowran et al.,
86 2004). The Cenozoic post-rift sedimentation is represented by the Wangerrip Group (late
87 Palaeocene to middle Eocene, mainly siliciclastic rich), the Nirranda Group (middle Eocene to early
88 Oligocene, mainly containing sandstones and marls), the Heytesbury Group (late Oligocene to late
89 Miocene, mainly contains marls and limestones), and the Whalers Bluff Formation (WBF; Pliocene-
90 Recent, mainly contains a mixed siliciclastic-carbonate sediments) (Figure 3a; Dickinson et al., 2002;
91 Krassay et al., 2004; Holford et al., 2014). Our study interval lies in the WBF formation at a time
92 when the study area was in a passive continental margin setting. In the continental slope area,
93 thick, localised sediments deposited in the Pliocene-recent succession, representing marine clastic
94 sediments deposited in submarine canyons (Figure 3b, 3c) (Tassone et al., 2011).

95 2.3 Oceanography

96 Two shelf-break currents dominate ocean circulation in the study area (Duran et al., 2020): (i) the
97 eastward-flowing South Australia Current (SAC) and (ii) the south-eastward-flowing Zeehan Current
98 (ZC) (Figure 2b). The SAC is an eastward-flowing current with high salinity and velocity (0.5 m/s),
99 originating from the centre of the Great Australian Bight Basin (Rochford, 1986). The current
100 operates down to 200 m depth (Middleton and Bye, 2007). The ZC is fed by the South Australian
101 Current, it is a poleward current with low salinity and high current velocity (0.4 m/s), flowing down
102 to 300 m water depth (Ridgway, 2007). The offshore area of the Otway Basin is also periodically
103 affected by seasonal hurricanes and storms (Holland and Gray, 1983; Kuleshov et al., 2002). The
104 above mentioned down-slope and along-slope marine oceanographic processes have jointly
105 influence the sedimentation in the Otway Basin.

106 As fluvial activity is limited in the study area (McGowran et al., 2004), the elongated mounded
107 seismic facies (sub-parallel to wavy, low- to high amplitude, internal truncations) in the WBF
108 Formation have a clear indication of contour current activity (Figure 3c). As similar seismic facies
109 have been interpreted as contourites that are affected by contourite currents in other submarine
110 settings (i.e. Stow and Faugères, 2008; Rebesco et al., 2014). Moreover, the modern canyons show
111 a clear eastward lateral migration compared to the buried Pliocene canyons in the continental shelf
112 region (Figure 3c). These observations all indicate that the overall eastward shelf break parallel

113 currents (SAC and LC) affect the sedimentary processes in the continental shelf region.

114 3. Dataset and Methodology

115 *3.1 Multibeam Dataset*

116 The multi-beam echosounder bathymetry data is provided by Geoscience Australia
117 (<https://portal.ga.gov.au/persona/marine>), covering an area of c. 12,000 km² (Figure 4a). The
118 lateral resolution of the data is 50 × 50 m, it enables the identification and interpretation of seafloor
119 morphology and associated canyons and MTCs, especially in areas absent of seismic-reflection data
120 (Figure 4a).

121 *3.2 Seismic Dataset*

122 The 3D pre-stack time migrated (PSTM) seismic-reflection data were acquired by Santos in 2002,
123 located in the vicinity of Portland, offshore SE Australia (Figure 2b). The survey covers an area of c.
124 360 km² with a bin spacing of 25 m × 12.5 m (inline × crossline), and a dominant frequency of 50
125 Hz at the seabed. The study estimates that the spatial resolution of the seismic data, given an
126 average velocity of the near seabed sediment derived from the seismic report (1824 m/s), is c. 9
127 m. The 3D seismic data are zero-phase, and presented in SEG normal polarity with an increase in
128 acoustic impedance expressed as a positive amplitude.

129 *3.3 Methodology*

130 The seismic-stratigraphic framework is correlated with Holford et al. (2014) work in an adjacent
131 area. Seismic and multi-beam data are used to map MTC and canyon related features. The key
132 morphometric parameters of the canyons (i.e. canyon width and height) are quantitatively
133 measured and discussed to reveal the sedimentary processes involved in the canyon origin and
134 evolution. In this study, the canyon width is defined as the distance between the canyon shoulders
135 (the point at which the canyon margin begins to dip away from the canyon axis; Laberg et al., 2000)
136 (Figure 5). The canyon height is defined as the depth from the canyon shoulder to the canyon base
137 (Figure 5).

138 4. Result

139 4.1 Morphology of the seafloor

140 The study area spans from the continental shelf, to slope, to abyssal plain environment (Figure 4a).
141 The morphology of the study area is characterised as having a narrow (c. 7km) and steep slope
142 (Figure 4b). The continental shelf area dips from 0.4° to 1° with an average water depth of 250 m
143 (Figure 4b). The continental slope area is characterised by a relatively gentle slope of c. 10° in the
144 upper section, to a steep slope gradient of c. 30° near the lower section, with water depths ranging
145 from 600 m to 1500 m, respectively (Figure 4b). The multi-beam reveals several canyons initiated
146 from the continental shelf region, spanning the continental slope, and ultimately terminating in
147 the abyssal plain (Figure 4a). Widely-distributed MTCs and their associated headwall scarps and
148 lateral margins have also been identified, and have a close relationship with the canyons (Figure
149 4a). The topographic profiles extracted from the multi-beam data in the abyssal plain show
150 dramatic differences in the across-canyon margin morphology (Figure 4c). In the abyssal plain,
151 where the seafloor gradient is relatively low (<2°), the width and height of the canyons (i.e. Canyon-
152 a and Canyon-b) increase along with the dip of the slope, with canyons converging at the deeper
153 section of the abyssal plain (Figure 4c, 4d). The width and the height of the canyon increases from
154 c. 5.6- 6.6 km to c. 10.9 km, and c. 300 m to 360 m, respectively (Figure 4c, 4d). The multibeam
155 data used in this study can only investigate the seafloor morphological features with a relatively
156 limited lateral resolution (c. 50 m). It lacks the ability to examine the detailed seafloor structures
157 in 3D and to reveal the characteristics of the buried sediments. Therefore, in the following section,
158 this study use high-resolution seismic reflection datasets to investigate the cause of the canyon
159 converging process, as well as the sedimentary process interactions between canyons and MTCs.

160 4.2 MTCs and canyons

161 Three MTCs (MTC-1, MTC-2, and MTC-3) have been interpreted in the study area (Figure 6a, 6b).
162 Seismic data reveals several distinctive NNW-SSE oriented extensional-fault scarps, and NE-SW
163 oriented lateral scarps near the shelf-edge, and within the slope and abyssal plain (Figure 6b). The
164 arcuate NNW-SSE dipping extensional scarps are interpreted as MTC headwall scarps that mark the
165 updip part of an MTC, where extensional deformation dominates (Figure 6b; i.e. Bull et al., 2009).
166 The NE-SW dipping lateral scarps are interpreted as MTCs lateral margins that separate deformed

167 sediments (MTCs) from the undeformed seabed (Figure 6b; i.e. Frey Martinez et al., 2005; Bull et
168 al., 2009). Based on the orientation of headwall scarps and lateral margins, the MTCs are
169 predominately transported subparallel to the dip direction of the slope.

170 Seven major canyons (canyon 1-7) spanning from continental shelf to abyssal plain are observed
171 within the MTC influenced area (Figure 6a, 6b). They are oriented NNW-SSW on the continental
172 slope, sub-parallel to the dip direction of the slope. Canyon-1-3 and Canyon-7 are initiated from
173 shelf edge headwall scarps with clear landward incision features, while Canyon-4-6 are restricted
174 in the continental slope (Figure 6b).

175 *4.3 MTC-1*

176 In MTC-1, multiple headwall scarps (HS-1 to HS-5) and their associated lateral margins are observed
177 from the map view and the correlated seismic sections (Figure 7a, 7b). Headwall scarps are
178 recognised as upward concaved lineation with scallop-shaped geometry (Figure 7b). In the seismic
179 dip section, the headwalls are nested in a terraced style, showing a truncated reflector that cuts
180 through upslope sediments (Figure 8a). The heights and angles of the scarps vary considerably
181 throughout MTC-1, with the highest (c. 170 m) and steepest (c. 40°). HS-5 occurring in the upper
182 part of MTC-1 (Figure 8b). The other four headwall scarps (HS-4 to HS-1) are comparatively smaller
183 and gentler than HS-5, with similar morphology and distributed in the central part of the MTC-1
184 (Figure 8b-d). The middle part of MTC-1 has a hummocky seabed expression in map view and
185 contains chaotic and blocky seismic facies in seismic section (Figure 7b, 8a). A clear basal shear
186 surface with a gentle gradient (c. 3°) that separates the underlying layered seismic facies from the
187 overlying chaotic seismic facies has been observed below the HS-5 and HS-1 (Figure 8a). The
188 chaotic and blocky facies accumulated downdip to the HS-4 and HS-1, showing a wedge-shaped
189 geometry in seismic section (Figure 8a) and a fan shaped geometry in plain view (Figure 7b).

190 The presence of the backstepping stair shape geometry, the relative flat basal shear surface, and
191 the deposition of chaotic seismic facies near the distal part of HS-4, HS-3, and HS-2, suggests that
192 the initial failure started at the lowermost part of MTC-1 and propagated retrogressively towards
193 the upper slope area. Our study thus interpret multiple headwall scarps (HS-1 - HS-5) resulting from
194 multiple retrogressive failure events, such as recorded in the Storegga slide and other MTCs (i.e.
195 Bryn et al., 2005; Sawyer et al., 2009; Badhani et al., 2020). The occurrence of retrogressive failure
196 has resulted in linear to sinuous depression features in plan-view (Figure 7b), and small-scale faults

197 or fractures in seismic cross-section (see headwall scarps in Figure 8b-d).

198 *4.4 Canyons in MTC-1*

199 In the upper section of MTC-1, the canyon system comprises three tributaries (Canyon-1 to Canyon-
200 3; Figure 6b, 7b), which terminate to the scarps near the shelf edge (Figure 6b). Canyon-1 and -2
201 are developed in the NE part of MTC-1, while Canyon-3 is in the NW part (Figure 7b). Canyon 1-3
202 have more pronounced seabed erosion than MTC-1. Near the HS-5, clear seabed incision and
203 truncations can be observed in the seismic sections that image the canyons (Figure 8b). Canyons
204 1-3 have a linear geometry in map view. The cross-sectional geometry of canyons is generally U-
205 shaped, with a gently sloping base surface (c. 1°) and steep canyon sidewalls (c. 60°) (Figure 8b,
206 8c). Canyons 1-3 trend downslope from the continental shelf towards the HS-5 of MTC-1 and
207 converge near the HS-3 (the confluence point; Figure 7b, 7c), and ultimately converging into a
208 broad canyon after passing through HS-2, at a water depth 1522 m to 1595 m (Figure 7b, 8d).
209 Numerous crescentic bedforms and axial incisions are observed along the axis of Canyon 1-3
210 (Figure 7b, 7c). In the pre-confluence region (abyssal plain area), the Canyons 1-3 ranges from c.
211 100 m to c. 670 m wide and c. 20 m to 134 m high (Figure 9a, 9b). In the post-confluence area, the
212 width increases from c.370 m to c.1140 m, which is 2-3 times wider than that of in the pre-
213 confluence region (Figure 9a). The canyon height increases from c. 90 m to c. 140 m in the post-
214 confluence area, slightly larger than the canyons in the pre-confluence area (Figure 9b).
215 This stratigraphic relationship between canyons and MTC-1 indicate that the deposition of the
216 MTC-1 occurred prior to the initiation of canyons. The crescentic bedforms are possibly associated
217 with supercritical currents (i.e. Zhong et al., 2015), suggesting gravity flows are still being initiated,
218 and canyons are remaining active as a sediment pathway today. Quantitative analyses of the
219 canyons indicate a strong correlation exists between the canyon width/height with distance along
220 the different MTC-1 headwall scarps. The increase of the canyon's width and depth after the
221 confluence point (near the HS-3) indicate headwall scarps has played a key role in dictating the
222 canyon morphology and erosivity. The abrupt increase in canyon width after the confluence can be
223 interpreted as an increase in discharge, because the converged canyon can be subjected to gravity
224 flows from multi-sources (see similar process from Mitchell, 2004). Our study thus indicates the
225 topography within MTC-1 was established as a function of topographic confinement imposed by
226 the backstep headwall scarps. The existence of the headwall scarps can facilitate the canyon

227 widening and deepening process.

228 *4.5 MTC-2 and MTC-3*

229 MTC-2 was deposited at the west of the MTC-1 (Figure 6b). MTC-2 has an E-dipping main headwall
230 scarp located in the lower slope setting, a south-dipping western lateral margin, and its eastern
231 lateral margin has been eroded by the MTC-1 (Figure 10a, 10b). MTC-2 contains four internal
232 headwall scarps (HS-1 to HS-4; Figure 10b) and associated lateral margins. Along the proximal part
233 of the western lateral margin, the sidewall displays up to at least three levels of local retrogressive
234 failures that make the west lateral margin complexed (Figure 10b). The cross-cutting relationship
235 between MTC-1 and MTC-2 reveals MTC-2 occurred after the MTC-1. Similar to MTC-1, the multi-
236 headwall scarps are the result of the retrogressive failure events associated with the emplacement
237 of MTC-2. MTC-3 was deposited in the west of the study area (Figure 6b). Distinctive NNW-ESE
238 dipping headwall scarps can be only identified near the upper boundary of the MTC-3 (Figure 10b).
239 Scarps in MTC-3 are significantly less than those in the MTC-1 and MTC-2 (Figure 10b).

240 *4.6 Canyons in MTC-2*

241 Two canyons (Canyon-4 and Canyon-5) that initiated from the lower slope setting, incised across
242 MTC-2, with a little (c. <50 m height) bathymetric expression in plain view (Figure 10a, 10b). The
243 morphology of Canyon-4 is only visible in map view near the lower slope, and it loses surface
244 expression at the location of HS-4 (Figure 10b). Upslope from the Canyon-5 head, two channels are
245 observed from map view (Figure 10b). The morphology of Canyon-5 meanders around the
246 headwall scarps within MTC-2, being initially WNW-SE strike at the location of HS-4 and HS-3,
247 shifting to SE at the site of HS-2, and shifting again to an abrupt SW bend at HS-1 (Figure 10b). After
248 passing through HS-1, Canyon-5 is oriented southward (Figure 10b). Seismic profiles of canyon-5
249 reveal a U-shaped erosional feature, and the cross-sectional morphology keeps constant along the
250 canyon-5's pathway (Figure 11a-c). The width and height of canyon-5 have a constant variation
251 compared to Canyon-1 (Figure 11d). The upper reach of canyon-5 has a deeper incision and width
252 that can reach 76 m and 565 m, respectively. In the abyssal plain, the width of canyon-5 decreases
253 from 565 m to c. 370 m, and increases to 750 m after passing through HS-3 (Figure 11d). The width
254 of Canyon-5 drops sharply to 343 m after passing through HS-1. The height of the Canyon-5
255 constantly decreases from c. 58 m near the HS-4 to c. 44 m near the HS-1 (Figure 11d). In summary,
256 from the HS-4 to HS-1, the Canyon-5 becomes narrower and less incised.

257 Limited distribution of Canyon-4 indicates that the canyon incision has been isolated to the lower
258 slope. The rapid shifting of Canyon-5 pathway indicates the presence of headwall scarps can
259 influence and divert the canyon transport direction. Canyon-5 has a clear backstep (landward)
260 incision and relates to a shelf edge headwall by channels, and this might suggest Canyon-5 is still
261 active during the Holocene. Our study suggests with the headward incision associated with canyon-
262 5, once the canyon head connects to shelf-edge headwall scarps, it will grow into a 'mature' stage
263 akin to the canyons in MTC-1.

264 *4.7 Canyons in MTC-3*

265 Two canyons (Canyon-6 and Canyon-7) are observed in MTC-3. The morphology of Canyon-6 is only
266 visible close to the lower slope (Figure 10b). Further downslope, the Canyon-6 lose its morphology
267 in map view, and there is no visible canyon form in the seismic section as well (Figure 12c). The
268 canyon-7 has a tripartite, concave head that cut c.7 km landward into the shelf (Figure 10b). The
269 cross-sectional geometry of canyon-7 shows a clear V-shaped incision. However, this V-shaped
270 downcutting geometry is only constrained in the lower slope region (Figure 12a, 12b). The width
271 and the height of canyon-7 are constantly low in the abyssal plain, ranging from c. 120 m to 175 m
272 and c. 20 m to 50 m, respectively (Figure 12d).

273 Canyon-6 and Canyon-7 have a broad flat canyon floor, with less apparent signs of incised channels,
274 which might indicate that the flow contributes to the formation of canyons that have been largely
275 displaced due to the absence of headwall scarps. Moreover, due to the absence of the scarps,
276 Canyon-6 and Canyon-7 show a low sinuosity and a subparallel pathway. No major canyon diverting,
277 nor converging has been observed in the MTC-3 region (Figure 10b).

278 **5. Discussion**

279 *5.1 Origin of the canyons*

280 Based on the morphology and depositional process, submarine canyons can be classified into two
281 main types (Type I and Type II from Jobe et al., 2011). Type I canyons normally indent the shelf-
282 edge and are linked with a clear bathymetric connection to fluvial systems, receiving abundant
283 coarse-grained sediment supply and generating erosive canyon morphologies (Jobe et al., 2011).
284 Type II canyons normally indent the continental slope, but have no clear bathymetric connection

285 to fluvial systems (thus a low sediment supply), exhibiting smooth and aggradational morphologies
286 (Jobe et al., 2011). The study area is disconnected from the modern fluvial system (Leach and
287 Wallace, 2001), which indicates a limited sediment input at or near the canyon heads. The canyons
288 are thus sediment starved when compared to canyons connected with direct fluvial input (e.g. the
289 Type I canyons) or have a high supplies of coarse grained sediment (Smith et al., 2018). Similar
290 canyons (e.g. the Type II canyons) that being isolated from major river input, with linear
291 morphology of low sinuosity, have been documented from other margins (e.g. Harris and Whiteway,
292 2011; Jobe et al., 2011). The initiation of the type II canyons are connected to the local failures near
293 continental margins or slopes, which is independent of sediment input (i.e. river feed) and sea-
294 level fluctuation (i.e. Normandeau et al., 2014). Other triggers, such as a mixed constructions and
295 modification by turbidity and contour currents near the canyon heads, have also been suggested
296 to the initiation of Type II canyons (i.e. Jobe et al., 2011). As inferred by canyons in the South China
297 Sea (Zhu et al., 2010), and other submarine settings (i.e. Rebesco et al., 2007). In this study, the
298 morphology of the canyon heads is strictly constrained within the headwall scarps near the shelf
299 edge (Figure 13a, 13b). The spatial relation between the shelf-edge headwall scarps and canyon
300 heads suggests the initiation of canyons is closely related to these pre-existing, steep shelf-edge
301 headwall scarps. Moreover, as the contour current is active near the shelf-edge area, the
302 movement of the contour current along the topographically low scarps may induce local
303 turbulence and produce down-canyon sediment transportation (i.e. Fenner et al., 1971; Warratz et
304 al., 2019). Thus, our study suggests that the canyon systems in the study area are initiated by a
305 combination of multistage retrogressive failure events and contour current activity near the pre-
306 existing headwall scarps (Figure 13c). Although the study area lacks river-sourced sediments,
307 canyon heads can capture sediments from local failure events associated with gravity flows that
308 erode the seabed and form canyons downslope (Figure 13d) (see also similar process from Atlantic
309 canyons; Twichell and Roberts, 1982). Other factors, such as hurricanes, typhoons and tidal
310 currents occurring in the continental shelf area, may also contribute to canyon initiation (Shepard
311 et al., 1974; Sequeiros et al., 2019). Hurricanes and typhoons can trigger waves and currents, thus
312 resuspending and carrying sediment. These processes will directly play a role in initiating the
313 turbidity currents, which bring the sediments into the canyon heads and enhance the canyoning
314 process (Sequeiros et al., 2019). Tidal currents can act as an efficient force for reworking and

315 carrying sediments in submarine settings (Shepard et al., 1974). Tidal currents can thus transport
316 sediments into the canyon heads, especially at places where river input is missing.

317 *5.2 Role of retrogressive failure mechanism on canyon evolution*

318 The headwall scarp of MTCs play an essential role in capturing turbidity currents and facilitating
319 turbidity channelization in submarine settings, as proved by examples from previous seismic- and
320 outcrop-based studies (Loncke et al., 2009; Alves and Cartwright, 2010; Ito, 2013; Qin et al., 2017;
321 Li et al., 2020). The three MTCs presented in this study have indicated the spatial variation of
322 canyon morphology is linked with the MTCs morphometric characteristics. This study further splits
323 these MTCs into two types (Type-1 and Type-2; Table 1) based on their morphology. Type-1 MTCs
324 (e.g. MTC-1 and MTC-2) are characterised as having multiple internal headwall scarps, and the
325 Type-2 MTCs (e.g. MTC-3) are characterised with no visible internal headwall scarps. In the
326 following section, our study attempts to define the possible mechanisms influencing different types
327 of MTCs and their impact on canyon evolution.

328 For Type-1 MTCs, the retrogressive failure events associated with MTC-1 have left a pronounced
329 negative seafloor space that greatly changed the slope morphology and created a series of
330 localised seafloor 'ponding' accommodations along the pathway of submarine canyon systems. The
331 gravity-driven downslope processes are sensitive to the slope gradient variations, preferentially
332 deposited where the gradient decreases the most (Kneller et al., 2016). The varied hierarchies of
333 headwall scarps can therefore trap or divert subsequent turbidity currents and facilitate canyon
334 systems' incision and development. Though the headwall scarps within MTC-2 does not widen nor
335 deepen canyons that are transported through, they do play an essential role in changing the canyon
336 direction. Compared to Type-1 MTCs, the Type-2 provides a reversed example of how headwall
337 scarps influence the canyon evolution. Within MTC-3, due to the lack of internal headwall scarps,
338 and hence a lack of ability to trap or capture the turbidity currents that flow through. Though
339 Canyon-7 has connections to the shelf-edge headwall scarps, the scale of the canyon is smaller
340 than those in the other two MTCs (i.e. Canyon-3 in MTC-1; Figure 6a, 6b). Therefore, our study
341 indicates the retrogressive failure mechanism of MTCs is responsible for canyon deepening and
342 confluence process, which can greatly influence the morphology of the canyons.

343 *5.3 Other factors that may influence the evolution of the canyon*

344 The evolution of submarine canyons can also be influenced by many other geological factors,

345 including (i) regional tectonics (i.e. regionally distributed faults), which influence the sediments
346 strength, thus the susceptibility to erosion during the formation of canyons (Covault et al., 2007);
347 (ii) the sea-level variation, which can boost sediment input to canyon heads (Vail, 1977;
348 Posamentier et al., 1991); (iii) downslope and along-slope depositional processes (i.e. gravity flows
349 and contour currents), which erode seafloor and enlarge submarine canyons (Pratson and Coakley,
350 1996; He et al., 2014; Miramontes et al., 2020).

351 In this study, tectonics is unlikely to be of significance for canyon development due to the relatively
352 stable nature of the southern Australian continental margin. The absence of intense tectonics and
353 seismicity may thus have a significant role in the preconditioning of the widely distributed MTCs,
354 as seismicity can actually strengthen sediments and increase stability (i.e. Sawyer and DeVore,
355 2015; DeVore and Sawyer, 2016). Recent studies revealed that the canyon initiation process does
356 not necessarily depend on the sea-level rise and fall, as well-developed canyon systems have been
357 identified during the sea-level rise in many submarine settings (i.e. Xu et al., 2010; Paull et al., 2013;
358 Normandeau et al., 2015). In the study area, the modern canyons are contiguous with Pliocene
359 canyon systems, showing similar geometry and slightly eastward migrated distribution patterns.
360 The similarities between buried Pliocene and modern canyons indicate that the location and
361 distribution of modern canyons are an extension of the infilled Pliocene canyon systems. The
362 overall eastward canyon lateral migration during Pliocene-Recent is interpreted as related to an
363 eastward shelf break parallel paleocurrent (i.e. SAC or LC), which is still active near current-day
364 shelf-edge (Godfrey et al., 1986). Moreover, our study suggests that the types of the underlying
365 deposits can also influence the morphology of the canyons. For example, Canyon-1 to Canyon-3
366 deposit above the slope background deposits (Figure 8b), while Canyon-6 deposits above a buried
367 MTC (Figure 12c). The quantitative analyses reveal that the Canyon-1 to Canyon-3 (immediately
368 above background deposits) are tentatively larger than that of the Canyon-6 (immediately above
369 buried MTCs). This is interpreted as buried MTCs, which are normally more consolidated than
370 undeformed background slope deposits (i.e. Shipp, 2004; Sawyer, 2007; Wu et al., 2021). Thus, the
371 erosivity and scale of the Canyon-6 are smaller than other canyons.

372 *5.4 Canyon evolution model*

373 Our study attempts to build an updated model of canyon formation based on the models proposed
374 by Pratson and Coakley (1996) and Jobe et al. (2011) emphasising the role of headwall scarps

375 associated with the regional distributed MTCs. Our model consists of three phases, MTC deposition,
376 canyon initiation, and canyon transition.

377 *Phase 1: MTCs deposition*

378 Prevailing eastward-flowing contour currents are continuously depositing sediment near the shelf
379 edge (Figure 14a). Earthquakes (i.e. Bornhold and Prior, 1989), sediment overloading generated
380 overpressure (i.e. Dugan and Flemings, 2000), or tectonic oversteepening (i.e. Moscardelli et al.,
381 2006) may have triggered the initial failures in the lower slope setting. The initial failure creates an
382 open scarp, that leaves the sediments in the up-dip part unstable. As the gravitational strain
383 accumulates, the sediments that near the initial scarp weaken. A new extensional failure (the
384 second scarp) will occur behind the initial scarp once the sediments become weaker than the along
385 slope gravity-induced stress (Figure 14a). The failure process will continue up-dip until the final
386 balance between the shear strength of the slope sediments and the shear stress of the gravitational
387 forces (Sawyer et al., 2009). This retrogressive failure mechanism has left a series of headwall
388 scarps and lateral scarps on the continental shelf and slope. The scarp-rich environment represents
389 the initial phase of canyon initiation (Figure 14b).

390 *Phase 2: the initial stage of the canyon system*

391 The erosional processes near the headwall scarps have led to triangular-shaped canyon heads
392 (Figure 14c). The failed sediments associated with erosional processes near the shelf edge could
393 excavate the pre-existing headwall scarps and contribute to the initial sediment influx for canyon
394 initiation (see the similar process from Pratson and Coakley, 1996; Puga-Bernabéu et al., 2011).
395 Once the canyon has been initiated, sediments collapse from the canyon sidewalls (canyon flank
396 failures) forms downslope flowing turbidity currents, facilitating the canyon flushing process. The
397 failure events associated with headwall scarp and canyon sidewalls permitted the delivery of
398 enough material to enable canyon formation and downward incision. Thus, the initiation
399 mechanism for canyons is the failure of sediments at the headwall scarps of the continental shelf
400 and the downslope eroding flows (Figure 14c) (see also similar process documented by: Pratson
401 and Ryan, 1994; Pratson and Coakley, 1996; Armitage et al., 2010). The mounded shape geometry
402 contourites may fail periodically (e.g. due to seasonal hurricanes or typhoons, contourite deposits
403 creating slope over-steepening, or sediments overpressure generated by rapid deposition of fine-
404 grained contourites) creating local turbulence near the shelf-edge headwall scarps, which further

405 facilitate the formation of flows that carry sediments into the canyon heads (Figure 14b, 14c;
406 Sequeiros et al., 2019; Brackenridge et al., 2020; Gatter et al., 2020).

407 *Phase 3: transitional stage*

408 With the continuous failures near the shelf-edge headwall scarps, the canyon heads gradually
409 establish into triangular or dendritic shapes. These triangular or dendritic shape structures
410 facilitate canyon head capture and funnel larger volumes of sediments into the canyon, and the
411 canyoning process becomes self-propagating (Figure 14c). The failed sediments near the headwall
412 scarps in the continental shelf converged into the channel-shaped conduit that is acting as
413 catchment areas for the canyon evolution. Downward sediment gravity flow generated by the
414 failed sediments can contribute significantly to the ongoing canyon excavation and downslope
415 propagation (Popescu et al., 2004; Baztan et al., 2005). The presence of the headwall scarps on the
416 slope settings provided further acceleration and canyon tributary convergence. The canyons are
417 thus progressively propagating to the far side of the lower slope and abyssal plain.

418 *5.5 Implication*

419 Many studies have shown how submarine MTCs rugose top surface can capture/reroute
420 subsequent sediment pathways based on seismic data (Loncke et al., 2009; Ortiz-Karpf et al., 2015;
421 Qin et al., 2017) and outcrops (Armitage et al., 2009; Jackson and Johnson, 2009; Kneller et al.,
422 2016). These studies are examples of MTCs locates near the shelf edge where the sediment supply
423 is high. The rugose top surfaces developed along the upper surface of MTCs is caused by the
424 presence of the internal rafted blocks. The rugose topography can be healed quickly by subsequent
425 sand-rich turbidity currents or separate failures. Thus, MTCs have a direct influence in the location
426 and distribution of reservoirs and important implications for hydrocarbon exploration.

427 Conversely, our study documents MTCs in low sediment supply margins where large-scale
428 sediment bypass is missing. Our study showed strong evidence that the emplace of MTCs has
429 played a key role in influencing the morphology evolution of canyon systems. Our study develops
430 a generic model of the MTCs headwall scarps, as a function of triggering and influencing the
431 morphological evolution of canyons, thus controlling the sediment bypass from the shelf edge to
432 lower slope and further abyssal plain. Our study indicates that the retrogressive failure mechanism
433 can facilitate long-distance sediment transportation within canyon systems, and it may be a
434 common and important process in a submarine setting where modern river systems are absent.

435 Previous studies have revealed that the density of marine plastics in canyons are 2-3 times larger
436 than the adjacent slopes or shelves (Pham et al., 2014; Cau et al., 2017; Kane et al., 2020). The
437 plastic pollutants can be transported across the shelf by contour currents and delivered to
438 submarine canyon heads formed far from terrestrial input (i.e. 150 km away from the coastline;
439 Zhong and Peng, 2021). Therefore, canyons not only can act as a major conduit for delivering
440 sediments, but they can also receive and carry marine plastics from shallow marine into the deep
441 ocean (Kane et al., 2020).

442 In this study, the canyon heads are subjected to episodic turbidity currents. Therefore they can
443 receive sediments as well as plastics delivered by contour currents near the shelf edge (i.e. Kane et
444 al., 2020; Zhong and Peng, 2021). Moreover, as the MTCs can facilitate longer transport distance
445 of sediments and plastics within canyons into the deep ocean, plastics delivered by canyon systems
446 may thus have the ability to travel into the deep Southern Ocean, with associated environmental
447 impacts (Zhong and Peng, 2021). Therefore, a combination of a high-resolution bathymetry dataset
448 with manned submersible dives is needed to further study this subject. The high-resolution
449 bathymetry dataset can provide detailed imaging of the seafloor, and can better constrain the role
450 of MTCs play during the canyon evolution. The manned submersible dives can establish plastic
451 and/or microplastic density in the deeper marine region, which will help to understand and
452 mitigate against anthropogenic impacts on the marine environment.

453 6. Conclusion

454 This study uses multi-beam bathymetry and seismic reflection data to document how the
455 retrogressive failure mechanism of MTCs and related headwall scarps have influenced the origin,
456 geometry, and distribution of canyons in a coarse-grained sediment starved submarine setting. In
457 summary: (i) the emplacement of MTCs have left multi-scaled headwall scarps and lateral margins
458 on the continental margin and slope area, (ii) the local failures developed associated headwall
459 scarps near the continental shelf-edge have provided the initial sediment supply for canyon
460 evolution, (iii) the headwall scarps which developed in the slope setting may act as the preferential
461 pathways for sediment gravity flows, and facilitate canyon development, (iv) our study thus
462 indicates that retrogressive failure mechanism can facilitate long-distance sediment transportation

463 and marine plastics within canyon systems in starved submarine settings.

464 Acknowledgements

465 We thank Geoscience Australia for providing the seismic reflection and multi-beam data used in
466 this study. The first and the third author would like to thank the State Key Laboratory of Marine
467 Geology for its financial support.

468 Data Availability

469 The seismic reflection data (OS02 3D survey and OS02 2D survey) and bathymetric data used in this
470 study can be requested from the Geoscience Australia Repository [https://www.ga.gov.au/data-](https://www.ga.gov.au/data-pubs)
471 [pubs](https://www.ga.gov.au/data-pubs). The GEBCO_2014 bathymetry map can be downloaded from the Gridded Bathymetry Data
472 Repository <https://www.ngdc.noaa.gov/maps/autogrid/>.

473 Figure Captions

474 Figure 1. (a) Model showing the time evolution of retrogressively failed MTCs, modified from
475 Sawyer et al. (2009). (b) Schematic sketch showing the different stages of a retrogressive failure,
476 modified from Locat et al. (2011).

477 Figure 2. (a) Regional map of the study area. (b) Zoom in map of the study area showing the location
478 of the city Portland and the Otway Basin. The white lines represent 2D seismic reflection data, and
479 the red polygon represents the location of the 3D seismic reflection dataset. Shaded relief
480 GEBCO_2014 bathymetry map downloaded from <https://www.ngdc.noaa.gov/maps/autogrid/>.

481 Abbreviations for the Otway Basin are as follows: SAC: South Australia Current, ZC: Zeehan Current.

482 Figure 3. (a) Stratigraphic and basin event chart for the Otway Basin (modified after Krassay et al.,
483 2004), including lithology interpretation and major tectonic events. The Horizon H1 has been
484 correlated to the intra-Maastrichtian unconformity surface from Holford et al. (2014). The Horizon
485 H2 is correlated to the base of the WBF. (b) Regional along slope seismic section showing the overall
486 tectonic of the study area. See location from Figure 2b. (c) Regional seismic section that

487 perpendicular to the slope, showing the key seismic horizons (H1 to seabed) and canyon bearing
488 intervals. See location from Figure 2b.

489 Figure 4. (a) Multi-beam bathymetry map of the study area illustrating the seafloor morphology.
490 The red polygon stands for the location of 3D seismic data. The location of this figure is marked by
491 the black dashed line in Figure 2b. (b) Bathymetric profile along the slope direction, showing the
492 seafloor morphology of the continental shelf, the continental slope and the abyssal plain. (c)
493 Bathymetric profile crossing the abyssal plain, showing the cross-sectional morphology of two
494 canyon systems (Canyon-a and Canyon-b). (d) Bathymetric profile revealing the combination of the
495 two canyon systems. See location in Figure 4a.

496 Figure 5. Schematic diagram showing the morphological parameters used in the quantitative
497 analyses of the canyons, including the width and height. (a) Uninterpreted cross-section of the
498 canyon system. (b) Interpreted cross-section of the canyon system with parameters used in
499 quantitative analyses.

500 Figure 6. (a) Contoured seafloor map of the study area extracted from the 3D seismic reflection
501 data. (b) Schematic representation of seafloor geomorphologic interpreted from Figure 6a. See the
502 location of this figure from Figure 2b.

503 Figure 7. (a) Zoomed in contoured seafloor map showing the region of MTC-1. (b) Interpreted map
504 of Figure 7a, showing the major headwall scarps in MTC-1 and the location of Canyon-1, Canyon-2,
505 and Canyon-3. (c) 3D view of the canyon confluence geometry in MTC-1, and the crescentic
506 bedforms within canyons. See the location of Figure 7c in Figure 7b.

507 Figure 8. (a) The N-S oriented seismic section of MTC-1 shows backstep shaped headwall scarps
508 and MTC-1's basal shear surface. (b) Seismic cross-section cutting through HS-5 and HS-4, showing
509 the cross-section of the upper part of the Canyon-1, Canyon-2, and Canyon-3. (c) Seismic cross-
510 section cutting through HS-3, showing the cross-section of the proximal part of the Canyon-1,
511 Canyon-2, and Canyon-3. (d) Seismic cross-section cutting through HS-2 and HS-1, showing the
512 cross-section of the post confluence part of the canyon system in MTC-1. See the location of Figure
513 8a-d in Figure 7a.

514 Figure 9. (a) Width profile of the canyon system in MTC-1. (b) Height profile of the canyon system
515 in MTC-1.

516 Figure 10. (a) Zoomed in contoured seafloor map showing the location of MTC-2 and MTC-3. B)

517 Interpreted map of Figure 10a, showing the headwall scarps in MTC-2 and MTC-3, and the location
518 of Canyon-4, Canyon-5, Canyon-6, and Canyon-7.

519 Figure 11. (a) Seismic cross-section cutting through HS-5 and HS-4 of MTC-2, showing the upper
520 part of the Canyon-4 and Canyon-5. (b) Seismic cross-section cutting through HS-2 of MTC-2,
521 showing the proximal part of the Canyon-5. (c) Seismic cross-section cutting through MTC-2,
522 showing the distal part of Canyon-5. See the location of Figure 11a-c in Figure 10a. (d) Width and
523 height profile of the Canyon-5 in MTC-2.

524 Figure 12. (a) Seismic cross-section cutting through the headwall of MTC-3, showing the upper part
525 of the Canyon-7. (b) Seismic cross-section showing the proximal part of the Canyon-6 and Canyon-
526 7. (c) Seismic cross-section showing the distal part of Canyon-6 and Canyon-7. See the location of
527 Figure 12a-c in Figure 10a. (d) Width and height profile of the Canyon-7 in MTC-3.

528 Figure 13. (a) 3D view of seafloor morphology showing the head of Canyon-5 and Canyon-7, and
529 the headwall scarps occurring on the shelf-edge. See location in Figure 5a. (b) 3D view of seafloor
530 morphology showing the head of Canyon-3, and the headwall scarps occurring on the shelf-edge.
531 See the location of Figure 13a-b in Figure 6a. (c) Sketch of 2D view of seafloor morphology showing
532 the headwall collapse and the initial stage of canyon evolution on shelf-edge. (d) Sketch of 2D view
533 of seafloor morphology showing the formation of the canyons.

534 Figure 14. Schematic figure showing the evolution model of the canyon system in the study area.
535 (a) Schematic figure showing that the deposition of contourite drifts near the shelf-edge, and the
536 occurrence of slope attached MTCs and associated headwall scarps near the lower slope. (b)
537 Schematic figure showing that the retrogressively failed MTCs and widely distributed headwall
538 scarps in the continental shelf and slope settings. (c) Schematic figure showing that canyons were
539 captured, converged and re-directed by the pre-existing headwall scarps.

540 Table Caption

541 Table 1. Classifications of MTCs and their influence on the canyon evolution.

542 Reference

- 543 Alves, T.M., Cartwright, J.A., 2010. The effect of mass-transport deposits on the younger slope
544 morphology, offshore Brazil. *Marine and Petroleum Geology* 27, 2027-2036.
- 545 Antobreh, A.A., Krastel, S., 2006. Morphology, seismic characteristics and development of Cap Timiris
546 Canyon, offshore Mauritania: a newly discovered canyon preserved-off a major arid climatic region.
547 *Marine and Petroleum Geology* 23, 37-59.
- 548 Armitage, D.A., Piper, D.J., Mcgee, D.T., Morris, W.R., 2010. Turbidite deposition on the glacially
549 influenced, canyon-dominated Southwest Grand Banks Slope, Canada. *Sedimentology* 57, 1387-1408.
- 550 Armitage, D.A., Romans, B.W., Covault, J.A., Graham, S.A., 2009. The influence of mass-transport-deposit
551 surface topography on the evolution of turbidite architecture: the Sierra Contreras, Tres Pasos formation
552 (Cretaceous), southern Chile. *Journal of Sedimentary Research* 79, 287-301.
- 553 Badhani, S., Cattaneo, A., Dennielou, B., Leroux, E., Colin, F., Thomas, Y., Jouet, G., Rabineau, M., Droz,
554 L., 2020. Morphology of retrogressive failures in the Eastern Rhone interfluvium during the last glacial
555 maximum (Gulf of Lions, Western Mediterranean). *Geomorphology* 351, 106894.
- 556 Baztan, J., Berné, S., Olivet, J.-L., Rabineau, M., Aslanian, D., Gaudin, M., Réhault, J.-P., Canals, M., 2005.
557 Axial incision: The key to understand submarine canyon evolution (in the western Gulf of Lion). *Marine*
558 *and Petroleum Geology* 22, 805-826.
- 559 Bornhold, B.D., Prior, D.B., 1989. Sediment blocks on the sea floor in British Columbia fjords. *Geo-Marine*
560 *Letters* 9, 135.
- 561 Brackenridge, R.E., Nicholson, U., Sapiie, B., Stow, D., Tappin, D.R., 2020. Indonesian Throughflow as a
562 preconditioning mechanism for submarine landslides in the Makassar Strait. *Geological Society, London,*
563 *Special Publications* 500, 195-217.
- 564 Bryn, P., Berg, K., Forsberg, C.F., Solheim, A., Kvalstad, T.J., 2005. Explaining the Storegga slide. *Marine*
565 *and Petroleum Geology* 22, 11-19.
- 566 Bull, S., Cartwright, J., Huuse, M., 2009. A review of kinematic indicators from mass-transport complexes
567 using 3D seismic data. *Marine and Petroleum Geology* 26, 1132-1151.
- 568 Canals, M., Puig, P., de Madron, X.D., Heussner, S., Palanques, A., Fabres, J., 2006. Flushing submarine
569 canyons. *Nature* 444, 354-357.
- 570 Cau, A., Alvito, A., Moccia, D., Canese, S., Pusceddu, A., Rita, C., Angiolillo, M., Follesa, M.C., 2017.
571 Submarine canyons along the upper Sardinian slope (Central Western Mediterranean) as repositories
572 for derelict fishing gears. *Marine pollution bulletin* 123, 357-364.
- 573 Covault, J.A., Normark, W.R., Romans, B.W., Graham, S.A., 2007. Highstand fans in the California
574 borderland: The overlooked deep-water depositional systems. *Geology* 35, 783-786.
- 575 DeVore, J.R., Sawyer, D.E., 2016. Shear strength of siliciclastic sediments from passive and active margins
576 (0–100 m below seafloor): insights into seismic strengthening, Submarine Mass Movements and their
577 Consequences. Springer, pp. 173-180.
- 578 Dickinson, J.A., Wallace, M.W., Holdgate, G.R., Gallagher, S.J., Thomas, L., 2002. Origin and timing of the
579 Miocene-Pliocene unconformity in southeast Australia. *Journal of Sedimentary Research* 72, 288-303.
- 580 Dugan, B., Flemings, P.B., 2000. Overpressure and fluid flow in the New Jersey continental slope:
581 Implications for slope failure and cold seeps. *Science* 289, 288-291.
- 582 Duran, E.R., Phillips, H.E., Furue, R., Spence, P., Bindoff, N.L., 2020. Southern Australia Current System

583 based on a gridded hydrography and a high-resolution model. *Progress in Oceanography* 181, 102254.
584 Farre, J.A., McGregor, B.A., Ryan, W.B., Robb, J.M., 1983. Breaching the shelfbreak: passage from
585 youthful to mature phase in submarine canyon evolution.
586 Fenner, P., Kelling, G., Stanley, D.J., 1971. Bottom currents in Wilmington submarine canyon. *Nature*
587 *Physical Science* 229, 52-54.
588 Frey Martinez, J., Cartwright, J., Hall, B., 2005. 3D seismic interpretation of slump complexes: examples
589 from the continental margin of Israel. *Basin Research* 17, 83-108.
590 Gatter, R., Clare, M.A., Hunt, J.E., Watts, M., Madhusudhan, B., Talling, P.J., Huhn, K., 2020. A multi-
591 disciplinary investigation of the AFEN Slide: the relationship between contourites and submarine
592 landslides. Geological Society, London, Special Publications 500, 173-193.
593 Gibson, G.M., Totterdell, J., White, L.T., Mitchell, C., Stacey, A., Morse, M., Whitaker, A., 2013. Pre-
594 existing basement structure and its influence on continental rifting and fracture zone development
595 along Australia's southern rifted margin. *Journal of the Geological Society* 170, 365-377.
596 Godfrey, J., Vaudrey, D., Hahn, S., 1986. Observations of the shelf-edge current south of Australia, winter
597 1982. *Journal of Physical Oceanography* 16, 668-679.
598 Gong, C., Wang, Y., Zhu, W., Li, W., Xu, Q., Zhang, J., 2011. The Central Submarine Canyon in the
599 Qiongdongnan Basin, northwestern South China Sea: architecture, sequence stratigraphy, and
600 depositional processes. *Marine and petroleum Geology* 28, 1690-1702.
601 Green, A., Uken, R., 2008. Submarine landsliding and canyon evolution on the northern KwaZulu-Natal
602 continental shelf, South Africa, SW Indian Ocean. *Marine Geology* 254, 152-170.
603 Harris, P.T., Whiteway, T., 2011. Global distribution of large submarine canyons: Geomorphic differences
604 between active and passive continental margins. *Marine Geology* 285, 69-86.
605 He, Y., Zhong, G., Wang, L., Kuang, Z., 2014. Characteristics and occurrence of submarine canyon-
606 associated landslides in the middle of the northern continental slope, South China Sea. *Marine and*
607 *Petroleum Geology* 57, 546-560.
608 Holford, S.P., Tuitt, A.K., Hillis, R.R., Green, P.F., Stoker, M.S., Duddy, I.R., Sandiford, M., Tassone, D.R.,
609 2014. Cenozoic deformation in the Otway Basin, southern Australian margin: Implications for the origin
610 and nature of post-breakup compression at rifted margins. *Basin Research* 26, 10-37.
611 Holland, G.J., Gray, W.M., 1983. Tropical cyclones in the Australian/southwest Pacific region. Colorado
612 State University. Libraries.
613 Ito, M., 2013. The role of slump scars in slope channel initiation: a case study from the Miocene Jatiluhur
614 Formation in the Bogor Trough, West Java. *Journal of Asian Earth Sciences* 73, 68-86.
615 Jackson, C.A., Johnson, H.D., 2009. Sustained turbidity currents and their interaction with debrite-
616 related topography; Labuan Island, offshore NW Borneo, Malaysia. *Sedimentary Geology* 219, 77-96.
617 Jobe, Z.R., Lowe, D.R., Uchytel, S.J., 2011. Two fundamentally different types of submarine canyons along
618 the continental margin of Equatorial Guinea. *Marine and Petroleum Geology* 28, 843-860.
619 Kane, I.A., Clare, M.A., Miramontes, E., Wogelius, R., Rothwell, J.J., Garreau, P., Pohl, F., 2020. Seafloor
620 microplastic hotspots controlled by deep-sea circulation. *Science* 368, 1140-1145.
621 Kneller, B., Dykstra, M., Fairweather, L., Milana, J.P., 2016. Mass-transport and slope accommodation:
622 Implications for turbidite sandstone reservoirs. *AAPG Bulletin* 100, 213-235.
623 Krassay, A., Cathro, D., Ryan, D., 2004. A regional tectonostratigraphic framework for the Otway Basin.
624 Kuleshov, Y., De Hoedt, G., Wright, W., Brewster, A., 2002. Thunderstorm distribution and frequency in
625 Australia. *Australian Meteorological Magazine* 51, 145.

626 Laberg, J., Vorren, T., Dowdeswell, J., Kenyon, N., Taylor, J., 2000. The Andøya Slide and the Andøya
627 Canyon, north-eastern Norwegian–Greenland Sea. *Marine Geology* 162, 259-275.

628 Leach, A., Wallace, M., 2001. Cenozoic submarine canyon systems in cool water carbonates from the
629 Otway Basin, Victoria, Australia.

630 Lee, H.J., Locat, J., Desgagnés, P., Parsons, J.D., McAdoo, B.G., Orange, D.L., Puig, P., Wong, F.L., Dartnell,
631 P., Boulanger, E., 2007. Submarine mass movements on continental margins, *Continental margin
632 sedimentation: from sediment transport to sequence stratigraphy*. Citeseer, pp. 213-274.

633 Li, W., Alves, T.M., Rebesco, M., Sun, J., Li, J., Li, S., Wu, S., 2020. The Baiyun Slide Complex, South China
634 Sea: A modern example of slope instability controlling submarine-channel incision on continental slopes.
635 *Marine and Petroleum Geology* 114, 104231.

636 Li, W., Alves, T.M., Urlaub, M., Georgiopoulou, A., Klauke, I., Wynn, R.B., Gross, F., Meyer, M.,
637 Repschläger, J., Berndt, C., 2017. Morphology, age and sediment dynamics of the upper headwall of the
638 Sahara Slide Complex, Northwest Africa: Evidence for a large Late Holocene failure. *Marine Geology* 393,
639 109-123.

640 Locat, A., Leroueil, S., Bernander, S., Demers, D., Jostad, H.P., Ouehb, L., 2011. Progressive failures in
641 eastern Canadian and Scandinavian sensitive clays. *Canadian Geotechnical Journal* 48, 1696-1712.

642 Loncke, L., Gaullier, V., Droz, L., Ducassou, E., Migeon, S., Mascle, J., 2009. Multi-scale slope instabilities
643 along the Nile deep-sea fan, Egyptian margin: A general overview. *Marine and Petroleum Geology* 26,
644 633-646.

645 McAdoo, B., Pratson, L., Orange, D., 2000. Submarine landslide geomorphology, US continental slope.
646 *Marine Geology* 169, 103-136.

647 McGowran, B., Holdgate, G., Li, Q., Gallagher, S., 2004. Cenozoic stratigraphic succession in southeastern
648 Australia. *Australian Journal of Earth Sciences* 51, 459-496.

649 Micallef, A., Mountjoy, J.J., Canals, M., Lastras, G., 2012. Deep-seated bedrock landslides and submarine
650 canyon evolution in an active tectonic margin: Cook Strait, New Zealand, Submarine mass movements
651 and their consequences. Springer, pp. 201-212.

652 Middleton, J.F., Bye, J.A., 2007. A review of the shelf-slope circulation along Australia's southern shelves:
653 Cape Leeuwin to Portland. *Progress in Oceanography* 75, 1-41.

654 Miramontes, E., Eggenhuisen, J.T., Jacinto, R.S., Poneti, G., Pohl, F., Normandeau, A., Campbell, D.C.,
655 Hernández-Molina, F.J., 2020. Channel-levee evolution in combined contour current–turbidity current
656 flows from flume-tank experiments. *Geology* 48, 353-357.

657 Mitchell, N.C., 2004. Form of submarine erosion from confluences in Atlantic USA continental slope
658 canyons. *American Journal of Science* 304, 590-611.

659 Moscardelli, L., Wood, L., 2008. New classification system for mass transport complexes in offshore
660 Trinidad. *Basin Research* 20, 73-98.

661 Moscardelli, L., Wood, L., 2016. Morphometry of mass-transport deposits as a predictive tool. *Bulletin*
662 128, 47-80.

663 Moscardelli, L., Wood, L., Mann, P., 2006. Mass-transport complexes and associated processes in the
664 offshore area of Trinidad and Venezuela. *AAPG bulletin* 90, 1059-1088.

665 Normandeau, A., Lajeunesse, P., St-Onge, G., 2015. Submarine canyons and channels in the Lower St.
666 Lawrence Estuary (Eastern Canada): Morphology, classification and recent sediment dynamics.
667 *Geomorphology* 241, 1-18.

668 Normandeau, A., Lajeunesse, P., St-Onge, G., Bourgault, D., Drouin, S.S.-O., Senneville, S., Belanger, S.,
669 2014. Morphodynamics in sediment-starved inner-shelf submarine canyons (Lower St. Lawrence

670 Estuary, Eastern Canada). *Marine Geology* 357, 243-255.

671 Nugraha, H.D., Jackson, C.A.-L., Johnson, H.D., Hodgson, D.M., Clare, M., 2019. How erosive are
672 submarine landslides?

673 Obelcz, J., Brothers, D., Chaytor, J., ten Brink, U., Ross, S.W., Brooke, S., 2014. Geomorphic
674 characterization of four shelf-sourced submarine canyons along the US Mid-Atlantic continental margin.
675 *Deep Sea Research Part II: Topical Studies in Oceanography* 104, 106-119.

676 Ortiz-Karpp, A., Hodgson, D., McCaffrey, W., 2015. The role of mass-transport complexes in controlling
677 channel avulsion and the subsequent sediment dispersal patterns on an active margin: the Magdalena
678 Fan, offshore Colombia. *Marine and Petroleum Geology* 64, 58-75.

679 Paull, C., Caress, D., Lundsten, E., Gwiazda, R., Anderson, K., McGann, M., Conrad, J., Edwards, B.,
680 Sumner, E., 2013. Anatomy of the La Jolla submarine canyon system; offshore Southern California.
681 *Marine Geology* 335, 16-34.

682 Perincek, D., Cockshell, C., 1995. The Otway basin: early Cretaceous rifting to Neogene inversion. *The*
683 *APPEA Journal* 35, 451-466.

684 Pham, C.K., Ramirez-Llodra, E., Alt, C.H., Amaro, T., Bergmann, M., Canals, M., Company, J.B., Davies, J.,
685 Duineveld, G., Galgani, F., 2014. Marine litter distribution and density in European seas, from the shelves
686 to deep basins. *PLoS one* 9, e95839.

687 Popescu, I., Lericolais, G., Panin, N., Normand, A., Dinu, C., Le Drezen, E., 2004. The Danube submarine
688 canyon (Black Sea): morphology and sedimentary processes. *Marine Geology* 206, 249-265.

689 Posamentier, H., Erskine, R., Mitchum, R., 1991. Models for submarine-fan deposition within a
690 sequence-stratigraphic framework, Seismic facies and sedimentary processes of submarine fans and
691 turbidite systems. Springer, pp. 127-136.

692 Posamentier, H.W., Martinsen, O.J., 2011. The character and genesis of submarine mass-transport
693 deposits: insights from outcrop and 3D seismic data. *Mass-transport deposits in deepwater settings:*
694 *Society for Sedimentary Geology (SEPM) Special Publication* 96, 7-38.

695 Pratson, L.F., Coakley, B.J., 1996. A model for the headward erosion of submarine canyons induced by
696 downslope-eroding sediment flows. *Geological Society of America Bulletin* 108, 225-234.

697 Pratson, L.F., Ryan, W.B., 1994. Pliocene to recent infilling and subsidence of intraslope basins offshore
698 Louisiana. *AAPG bulletin* 78, 1483-1506.

699 Puga-Bernabéu, Á., Webster, J.M., Beaman, R.J., Guilbaud, V., 2011. Morphology and controls on the
700 evolution of a mixed carbonate–siliciclastic submarine canyon system, Great Barrier Reef margin, north-
701 eastern Australia. *Marine Geology* 289, 100-116.

702 Qin, Y., Alves, T.M., Constantine, J., Gamboa, D., 2017. The role of mass wasting in the progressive
703 development of submarine channels (Espírito Santo Basin, SE Brazil). *Journal of Sedimentary Research*
704 87, 500-516.

705 Rebesco, M., Camerlenghi, A., Volpi, V., Neagu, C., Accettella, D., Lindberg, B., Cova, A., Zgur, F., Party,
706 M., 2007. Interaction of processes and importance of contourites: insights from the detailed
707 morphology of sediment Drift 7, Antarctica. *Geological Society, London, Special Publications* 276, 95-
708 110.

709 Rebesco, M., Hernández-Molina, F.J., Van Rooij, D., Wåhlin, A., 2014. Contourites and associated
710 sediments controlled by deep-water circulation processes: State-of-the-art and future considerations.
711 *Marine Geology* 352, 111-154.

712 Ridgway, K., 2007. Seasonal circulation around Tasmania: an interface between eastern and western
713 boundary dynamics. *Journal of Geophysical Research: Oceans* 112.

714 Rochford, D., 1986. Seasonal changes in the distribution of Leeuwin Current waters of Southern
715 Australia. *Marine and Freshwater Research* 37, 1-10.

716 Sawyer, D.E., 2007. Lateral Variations in Core, Log, and Seismic Attributes of a Mass Transport Complex
717 in the Ursa Region, IODP Expedition 308, Northern Gulf of Mexico.

718 Sawyer, D.E., DeVore, J.R., 2015. Elevated shear strength of sediments on active margins: Evidence for
719 seismic strengthening. *Geophysical Research Letters* 42, 10,216-210,221.

720 Sawyer, D.E., Flemings, P.B., Dugan, B., Germaine, J.T., 2009. Retrogressive failures recorded in mass
721 transport deposits in the Ursa Basin, Northern Gulf of Mexico. *Journal of Geophysical Research: Solid*
722 *Earth* 114.

723 Sequeiros, O.E., Pittaluga, M.B., Frascati, A., Pirmez, C., Masson, D.G., Weaver, P., Crosby, A.R., Lazzaro,
724 G., Botter, G., Rimmer, J.G., 2019. How typhoons trigger turbidity currents in submarine canyons.
725 *Scientific reports* 9, 1-15.

726 Shepard, F.P., 1972. Submarine canyons. *Earth-Science Reviews* 8, 1-12.

727 Shepard, F.P., Dill, R.F., Dill, R.F., 1966. Submarine canyons and other sea valleys. Rand McNally.

728 Shepard, F.P., Marshall, N.F., McLoughlin, P.A., 1974. " Internal Waves" Advancing along Submarine
729 Canyons. *Science* 183, 195-198.

730 Shipp, R.C., 2004. Physical Characteristics and Impact of Mass Transport Complexes on Deepwater Jetted
731 Conductors and Suction Anchor Piles.

732 Smith, M.E., Werner, S.H., Buscombe, D., Finnegan, N.J., Sumner, E.J., Mueller, E.R., 2018. Seeking the
733 shore: Evidence for active submarine canyon head incision due to coarse sediment supply and focusing
734 of wave energy. *Geophysical Research Letters* 45, 12,403-412,413.

735 Stow, D., Faugères, J.-C., 2008. Contourite facies and the facies model. *Developments in sedimentology*
736 60, 223-256.

737 Stow, D.A., Mayall, M., 2000. Deep-water sedimentary systems: new models for the 21st century.
738 *Marine and Petroleum Geology* 17, 125-135.

739 Su, M., Lin, Z., Wang, C., Kuang, Z., Liang, J., Chen, H., Liu, S., Zhang, B., Luo, K., Huang, S., 2020.
740 Geomorphologic and infilling characteristics of the slope-confined submarine canyons in the Pearl River
741 Mouth Basin, northern South China Sea. *Marine Geology* 424, 106166.

742 Tassone, D., Holford, S., Tingay, M., Tuitt, A., Stoker, M., Hillis, R., 2011. Overpressures in the central
743 Otway Basin: the result of rapid Pliocene–Recent sedimentation? *The APPEA Journal* 51, 439-458.

744 Totterdell, J., Bradshaw, M., Owen, K., Hashimoto, T., Hall, L., 2014. Petroleum geology inventory of
745 Australia's offshore frontier basins. *Geoscience Australia*.

746 Twichell, D.C., Roberts, D.G., 1982. Morphology, distribution, and development of submarine canyons
747 on the United States Atlantic continental slope between Hudson and Baltimore Canyons. *Geology* 10,
748 408-412.

749 Urgeles, R., Camerlenghi, A., 2013. Submarine landslides of the Mediterranean Sea: Trigger mechanisms,
750 dynamics, and frequency–magnitude distribution. *Journal of Geophysical Research: Earth Surface* 118,
751 2600-2618.

752 Vail, P., 1977. Seismic stratigraphy and global changes of sea level. *Bull. Am. Assoc. Petrol. Geol., Mem.*
753 26, 49-212.

754 Warratz, G., Schwenk, T., Voigt, I., Bozzano, G., Henrich, R., Violante, R., Lantzsch, H., 2019. Interaction
755 of a deep-sea current with a blind submarine canyon (Mar del Plata Canyon, Argentina). *Marine Geology*
756 417, 106002.

757 Watson, S.J., Mountjoy, J.J., Crutchley, G.J., 2020. Tectonic and geomorphic controls on the distribution
758 of submarine landslides across active and passive margins, eastern New Zealand. Geological Society,
759 London, Special Publications 500, 477-494.

760 Weimer, P., Slatt, R.M., 2004. Petroleum systems of deepwater settings. Society of Exploration
761 Geophysicists and European Association of ...

762 Willcox, J., Stagg, H., 1990. Australia's southern margin: a product of oblique extension. Tectonophysics
763 173, 269-281.

764 Williams, S.C., 2016. News Feature: Skimming the surface of underwater landslides. Proceedings of the
765 National Academy of Sciences 113, 1675-1678.

766 Wu, N., Jackson, C.A.L., Johnson, H.D., Hodgson, D.M., Clare, M.A., Nugraha, H.D., Li, W., 2021. The
767 formation and implications of giant blocks and fluid escape structures in submarine lateral spreads.
768 Basin Research.

769 Xu, J., Swarzenski, P.W., Noble, M., Li, A.-C., 2010. Event-driven sediment flux in Hueneme and Mugu
770 submarine canyons, southern California. Marine Geology 269, 74-88.

771 Zhong, G., Cartigny, M.J., Kuang, Z., Wang, L., 2015. Cyclic steps along the South Taiwan Shoal and West
772 Penghu submarine canyons on the northeastern continental slope of the South China Sea. Bulletin 127,
773 804-824.

774 Zhong, G., Peng, X., 2021. Transport and accumulation of plastic litter in submarine canyons—The role
775 of gravity flows. Geology 49, 581-586.

776 Zhu, M., Graham, S., Pang, X., McHargue, T., 2010. Characteristics of migrating submarine canyons from
777 the middle Miocene to present: Implications for paleoceanographic circulation, northern South China
778 Sea. Marine and Petroleum Geology 27, 307-319.

779

780

Figure 1

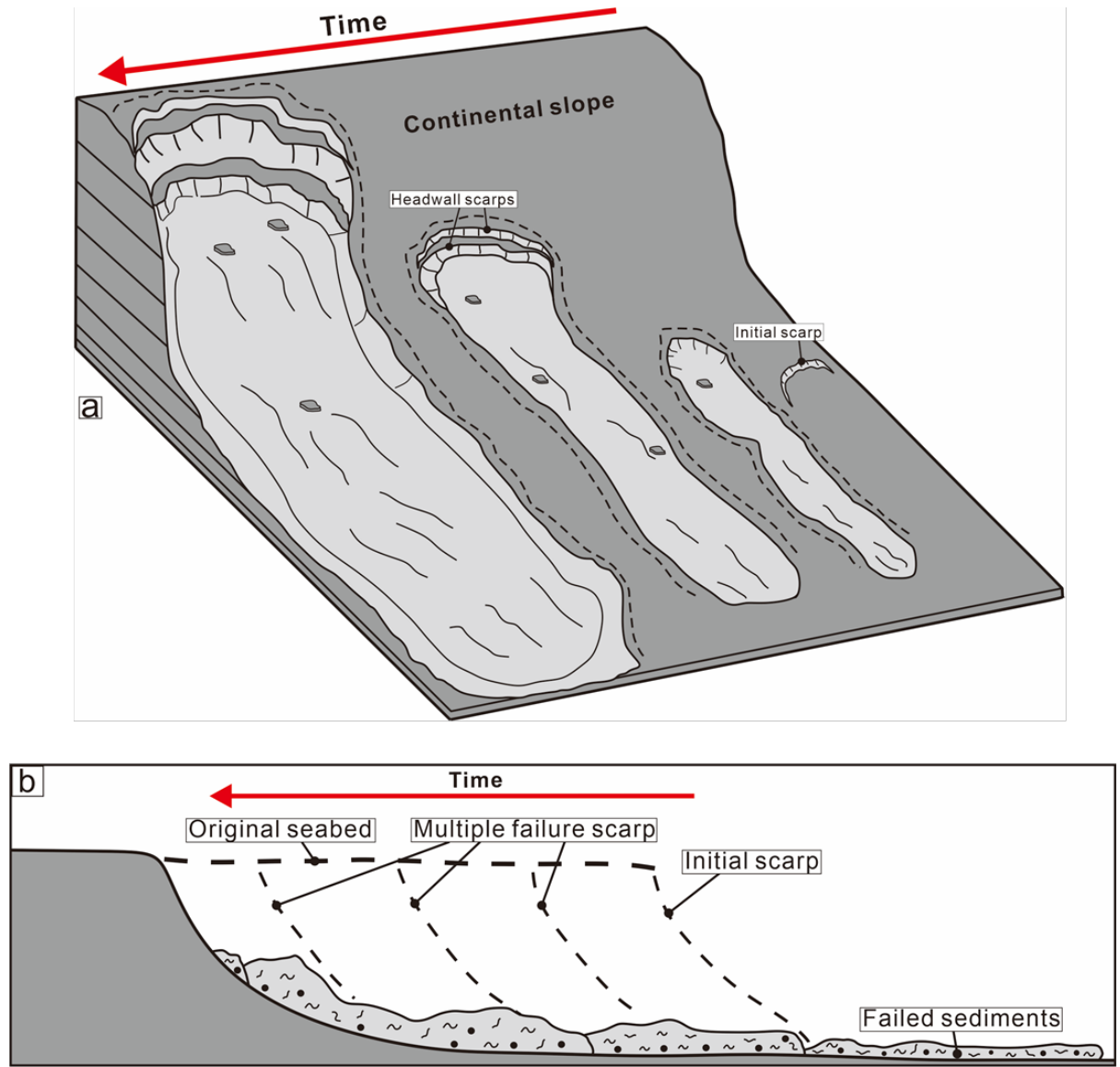


Figure 2

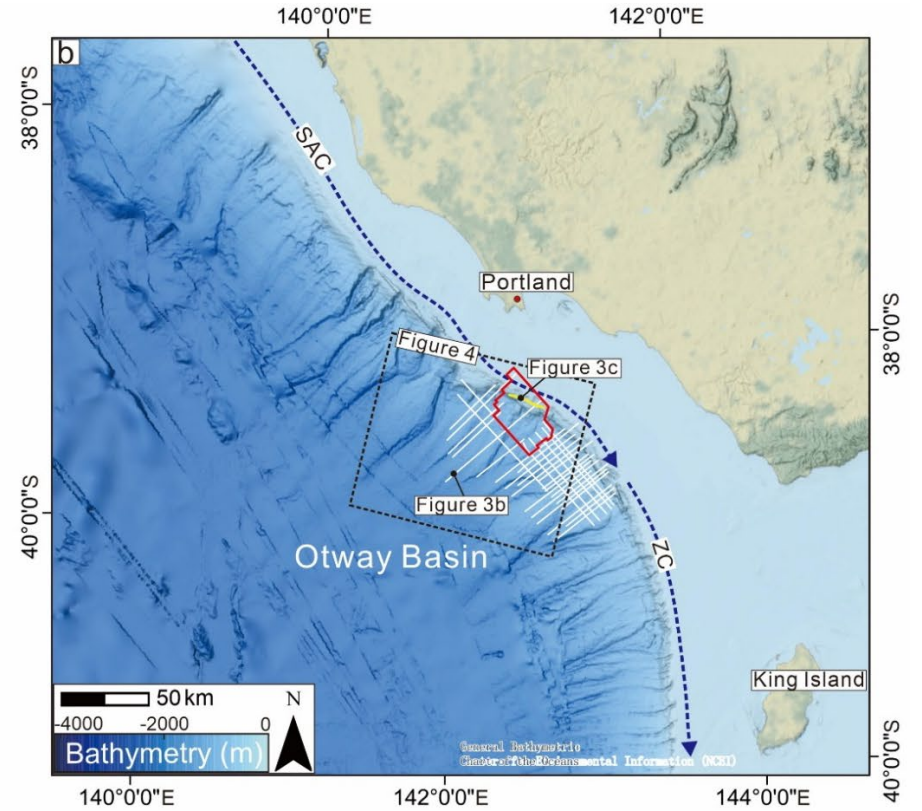
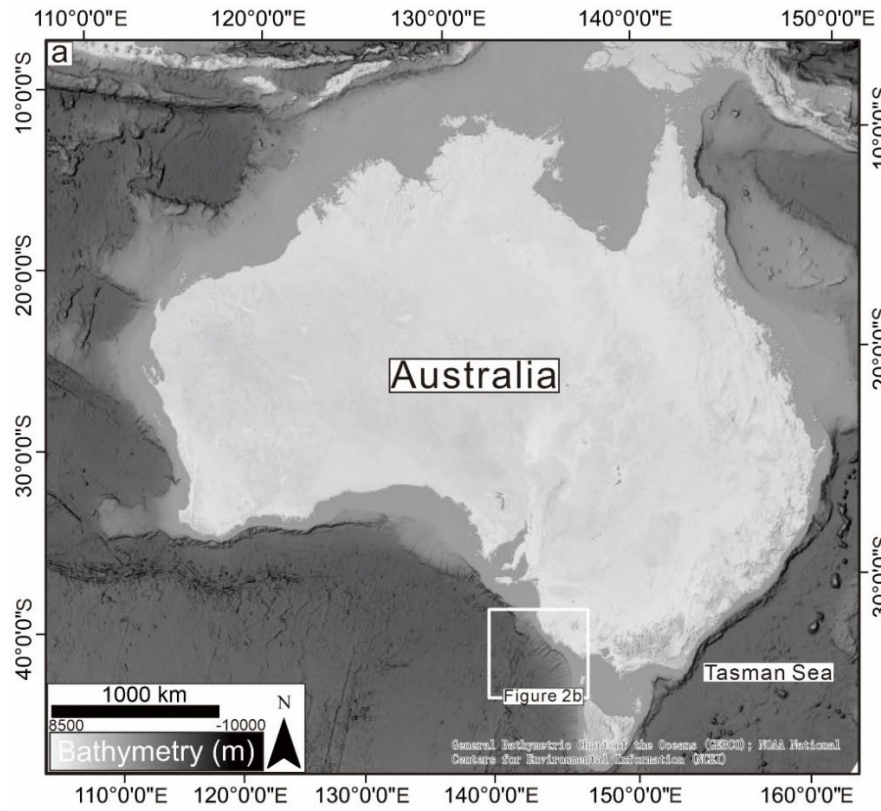


Figure 3

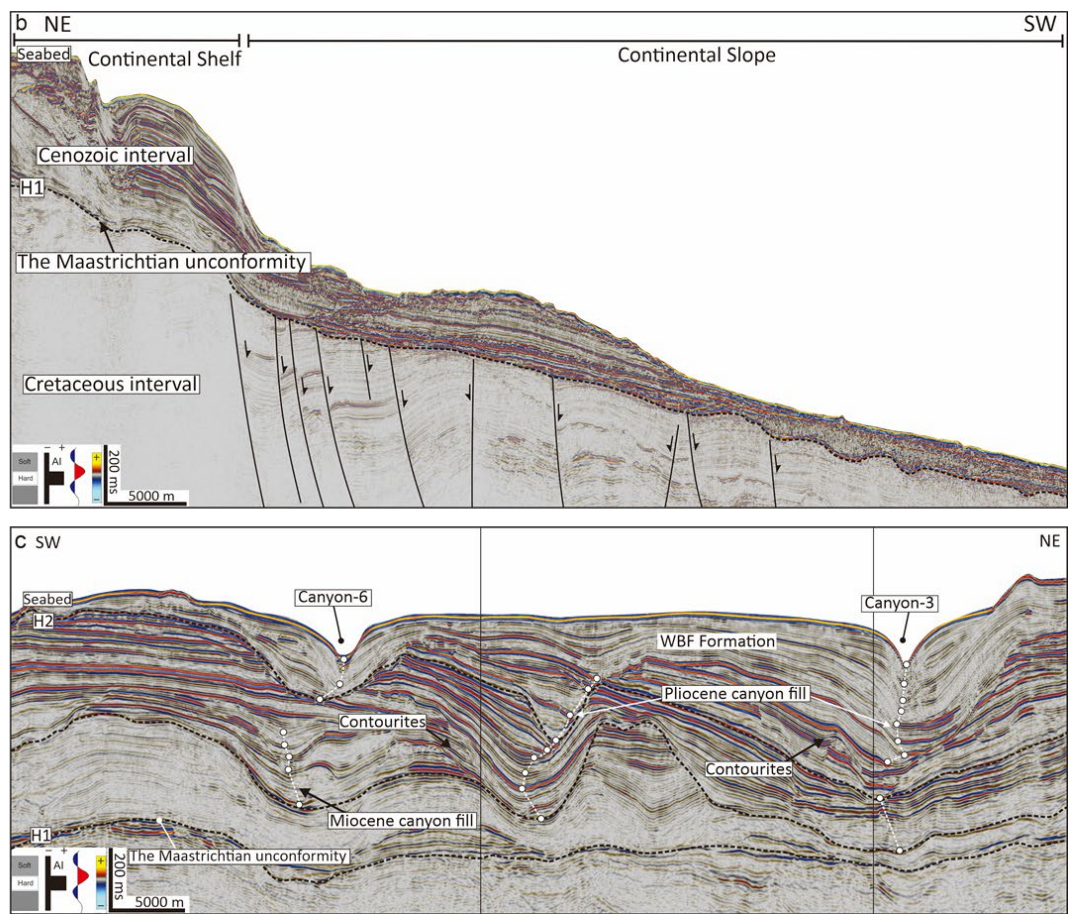
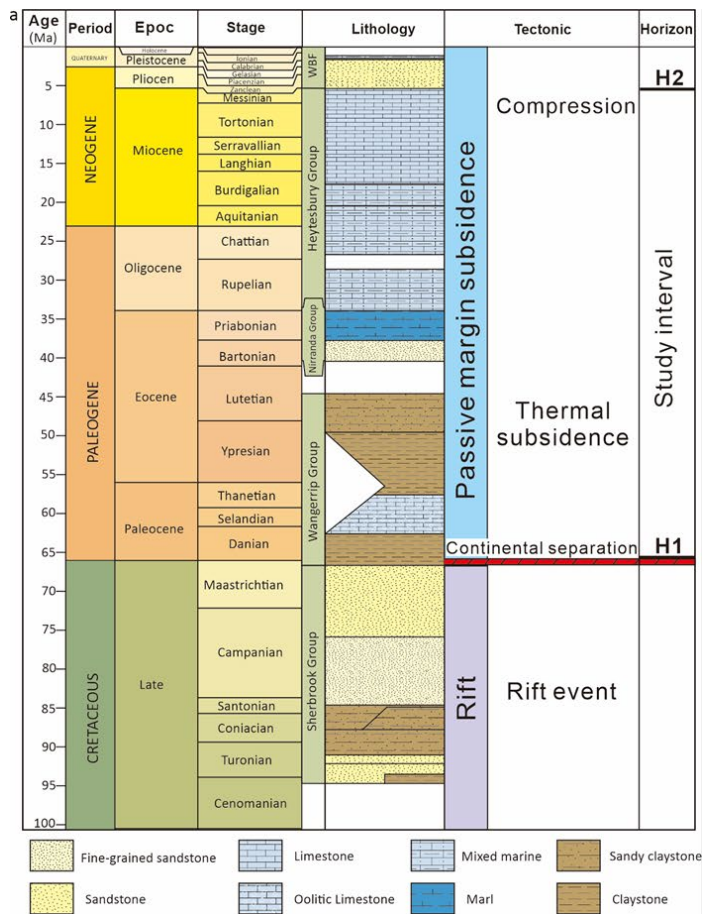


Figure 4

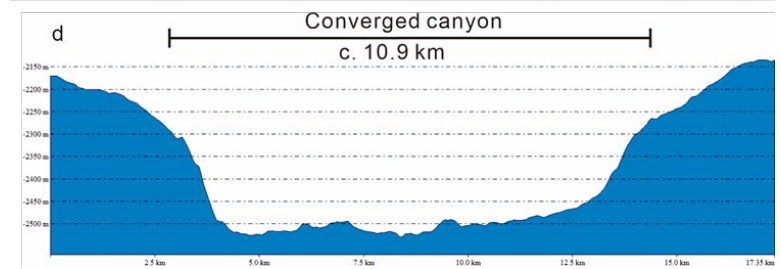
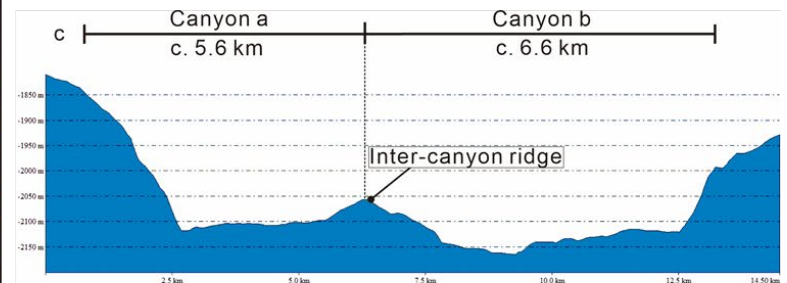
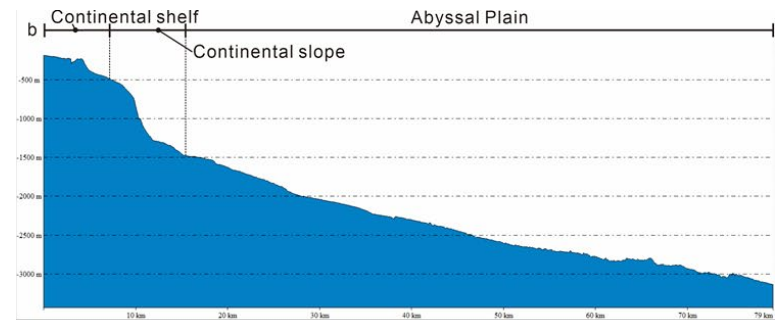
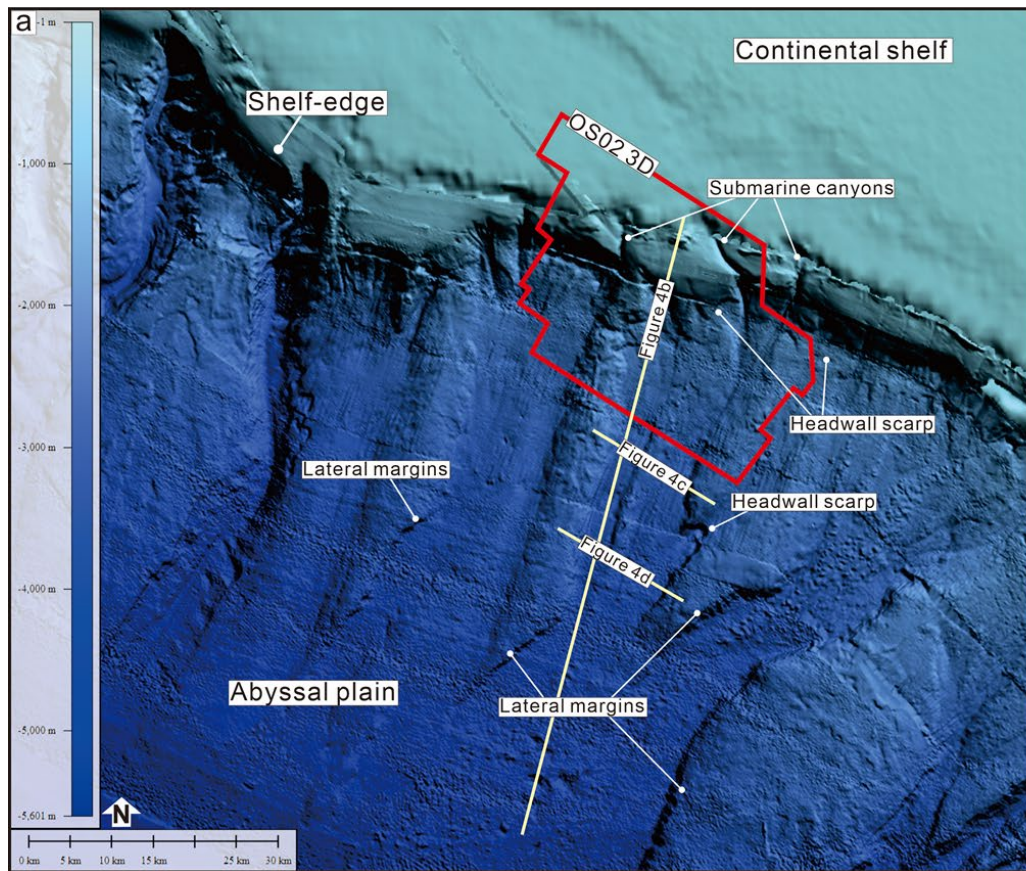


Figure 5

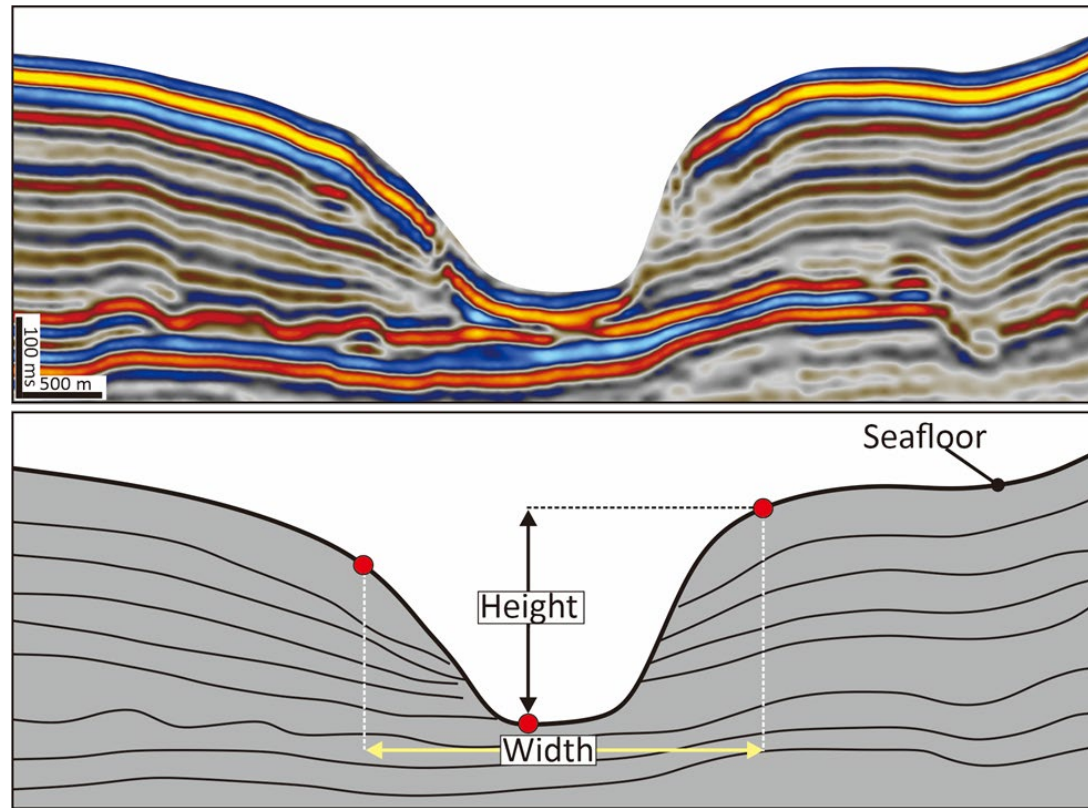


Figure 6

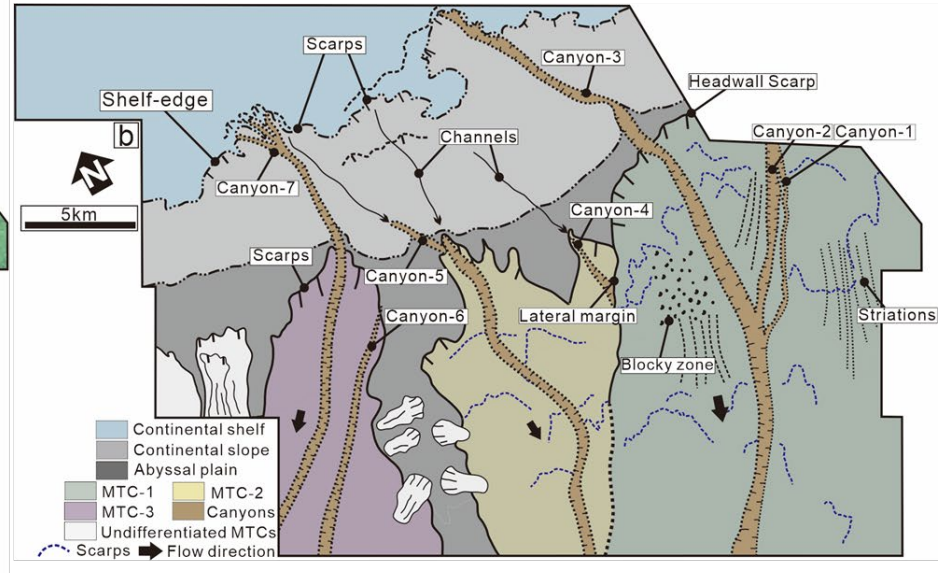
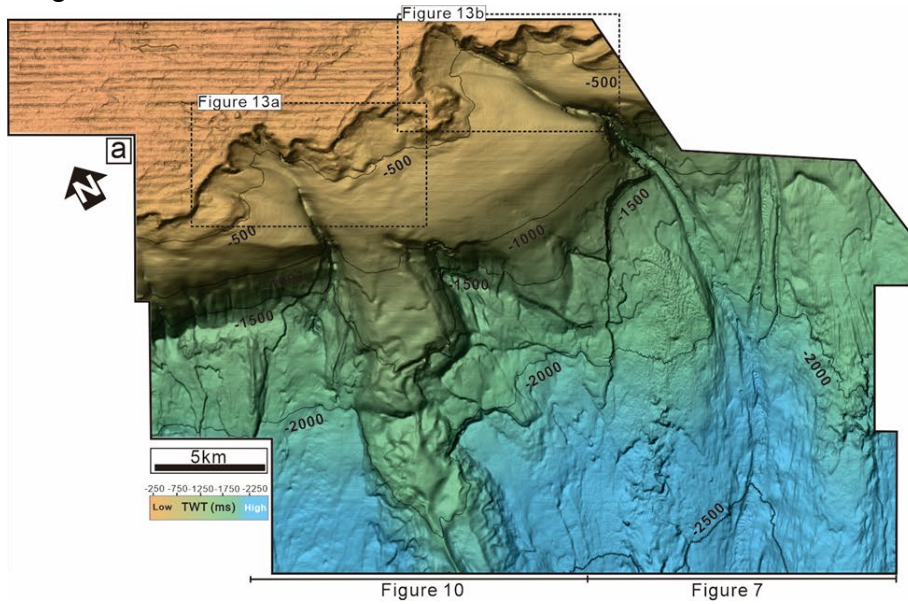
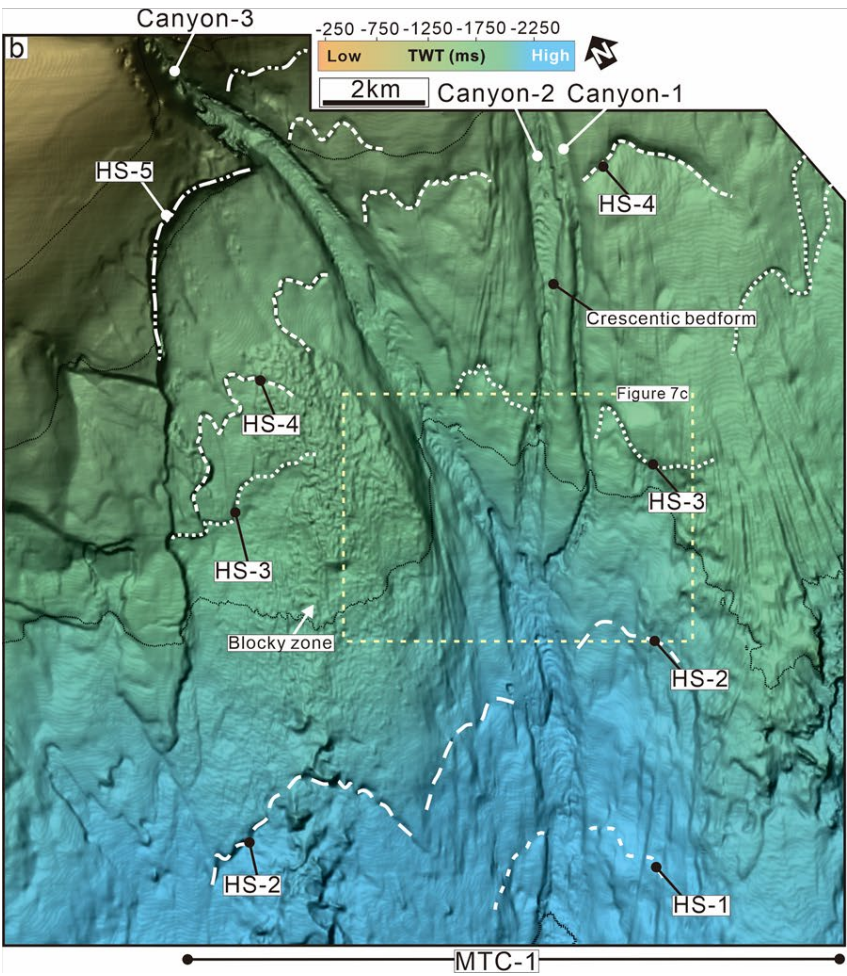
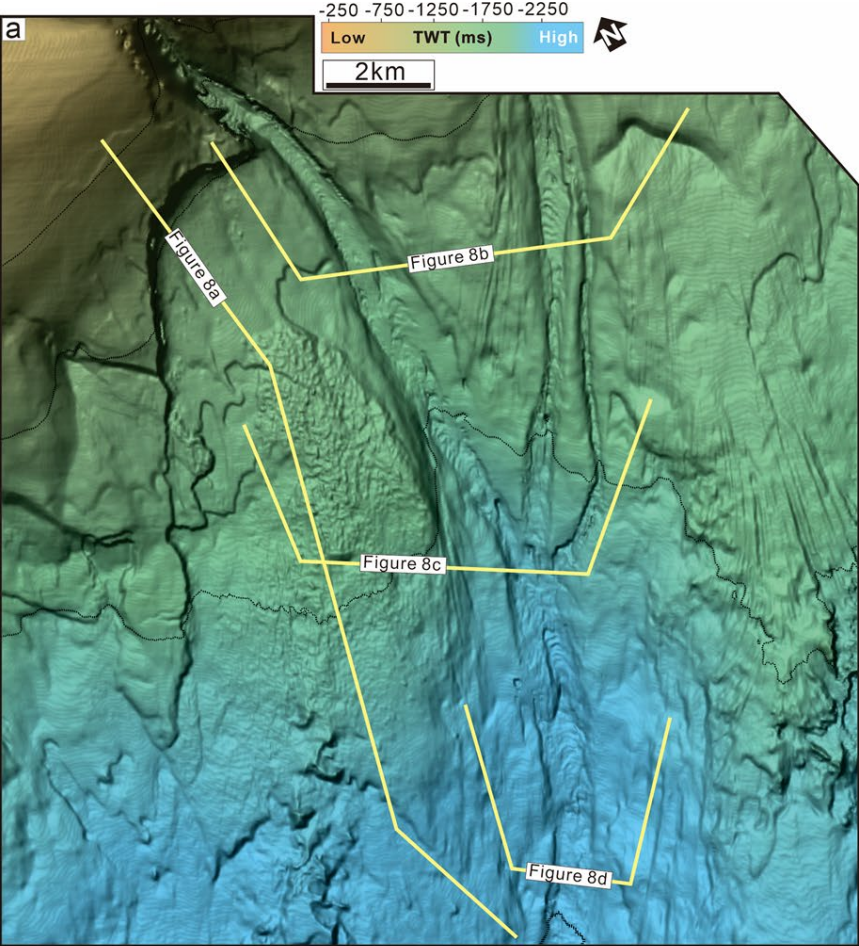


Figure 7



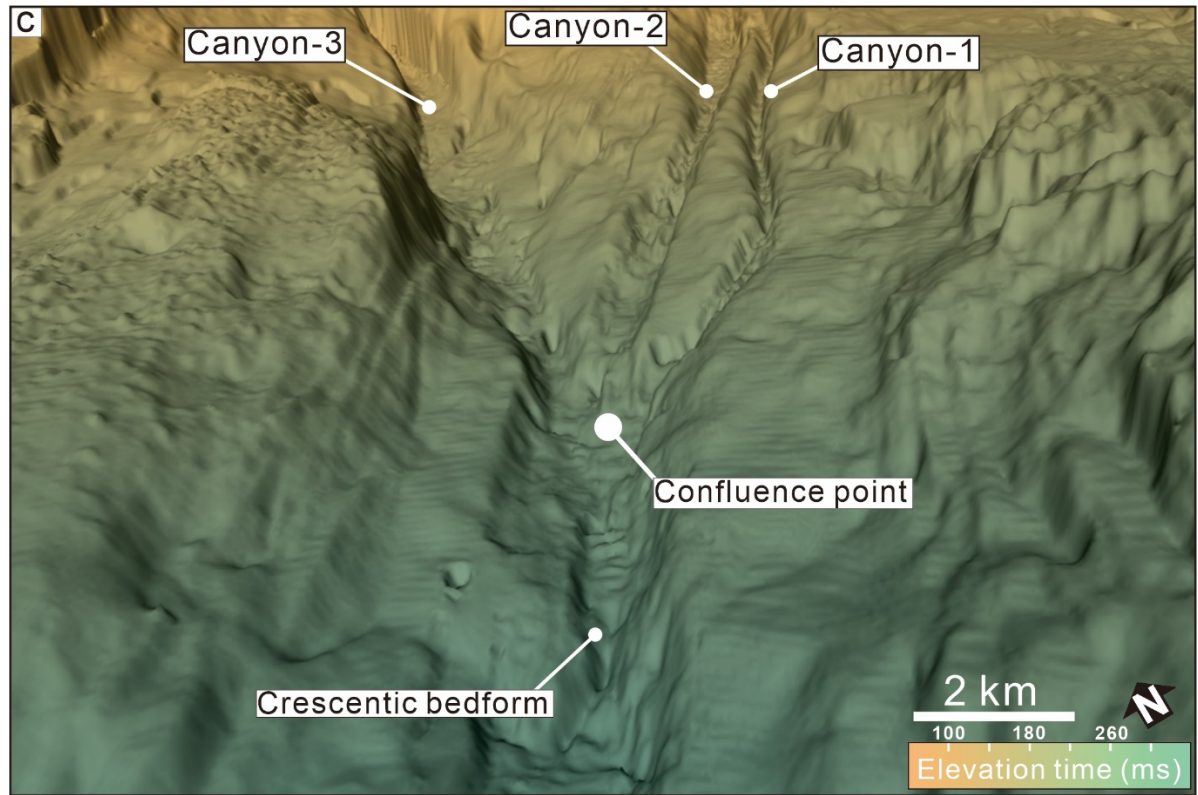


Figure 8

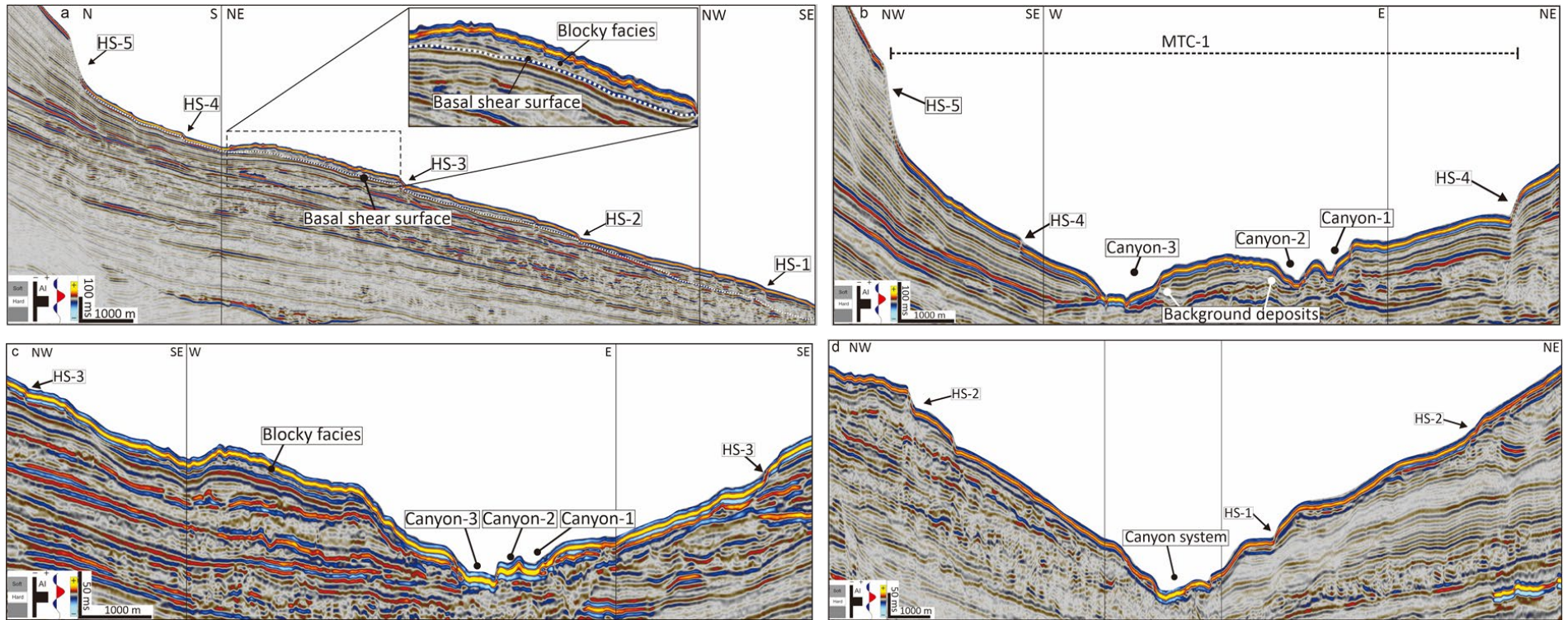


Figure 9

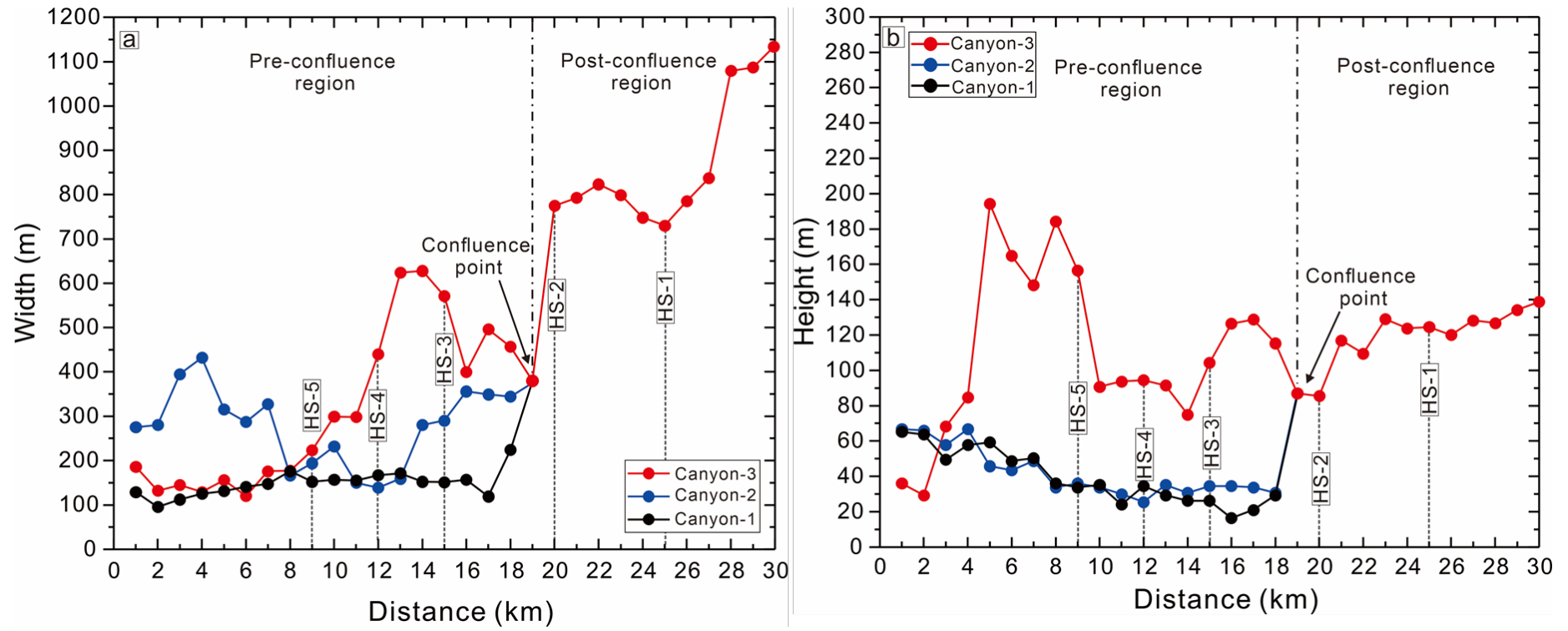


Figure 10

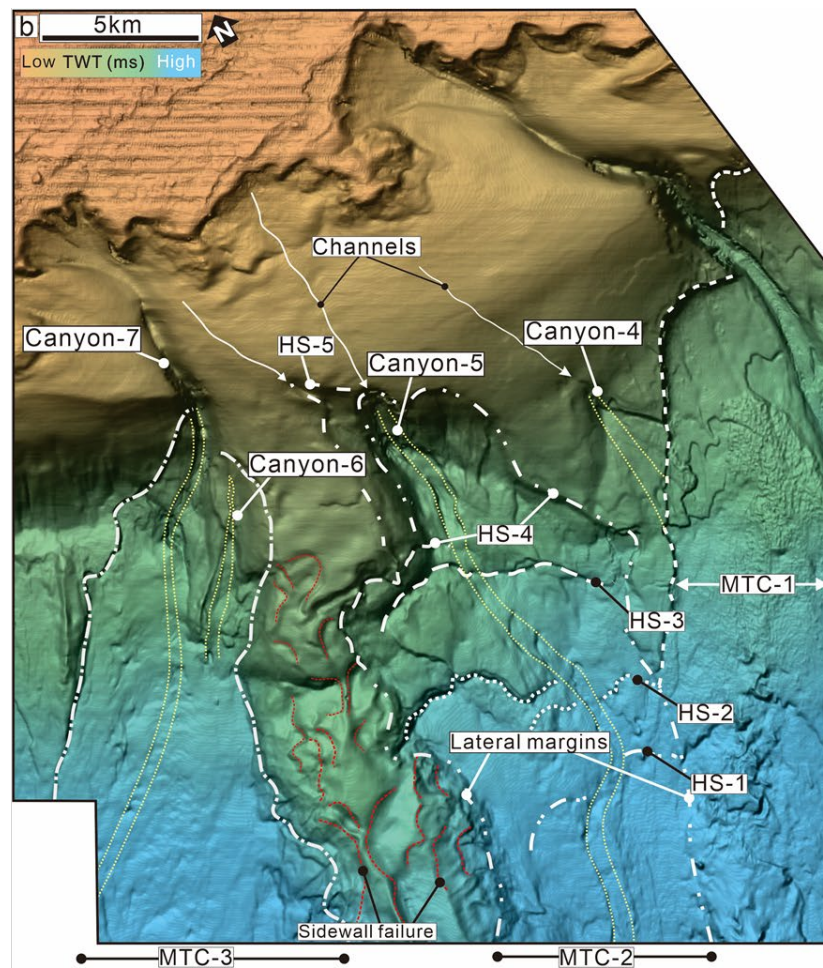
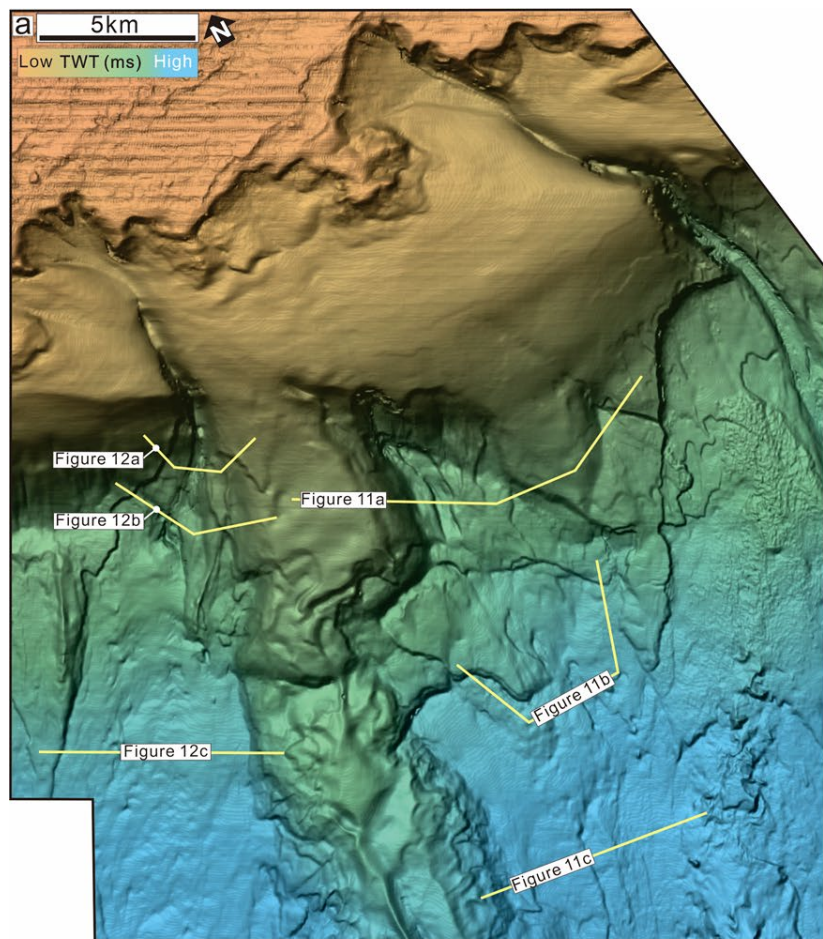


Figure 11

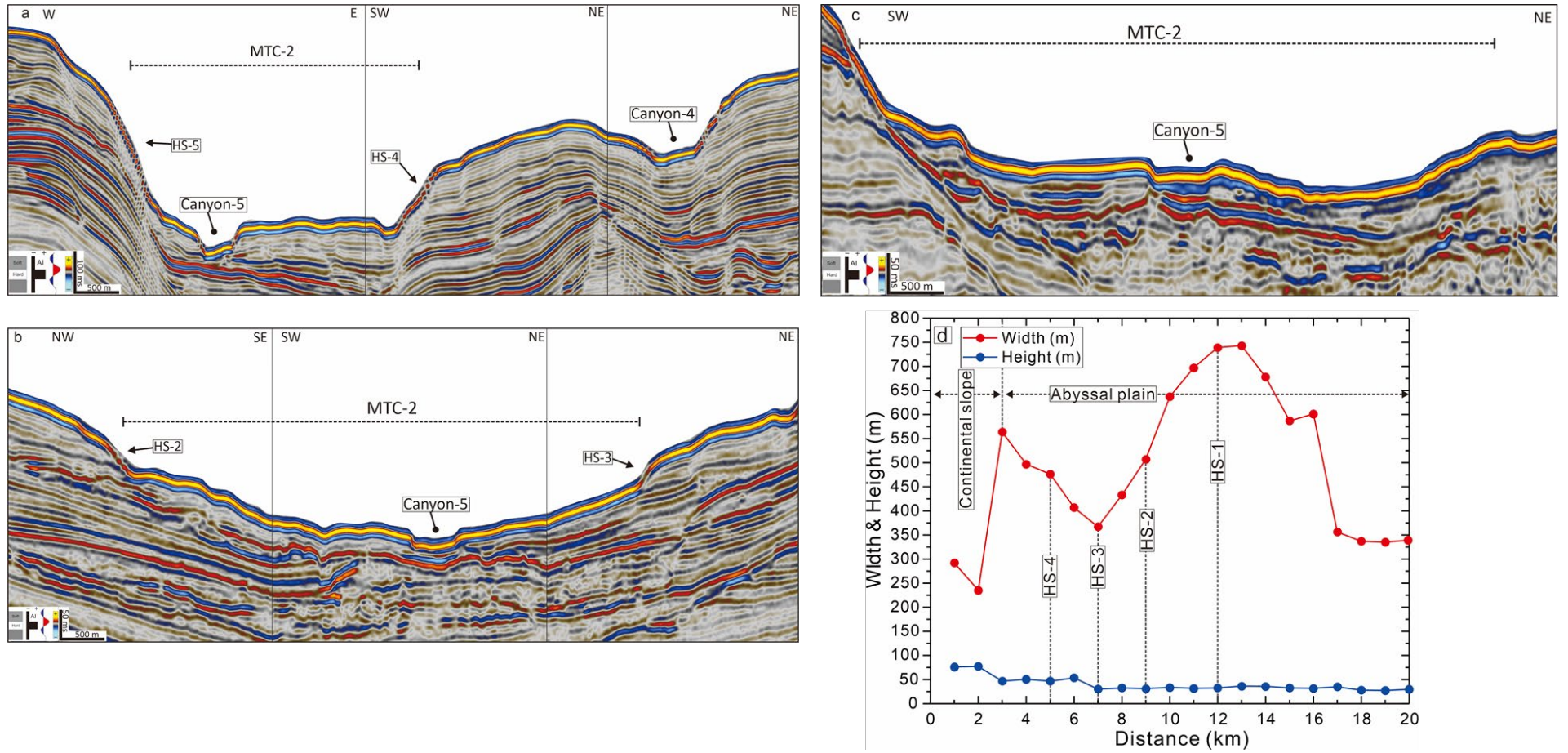


Figure 12

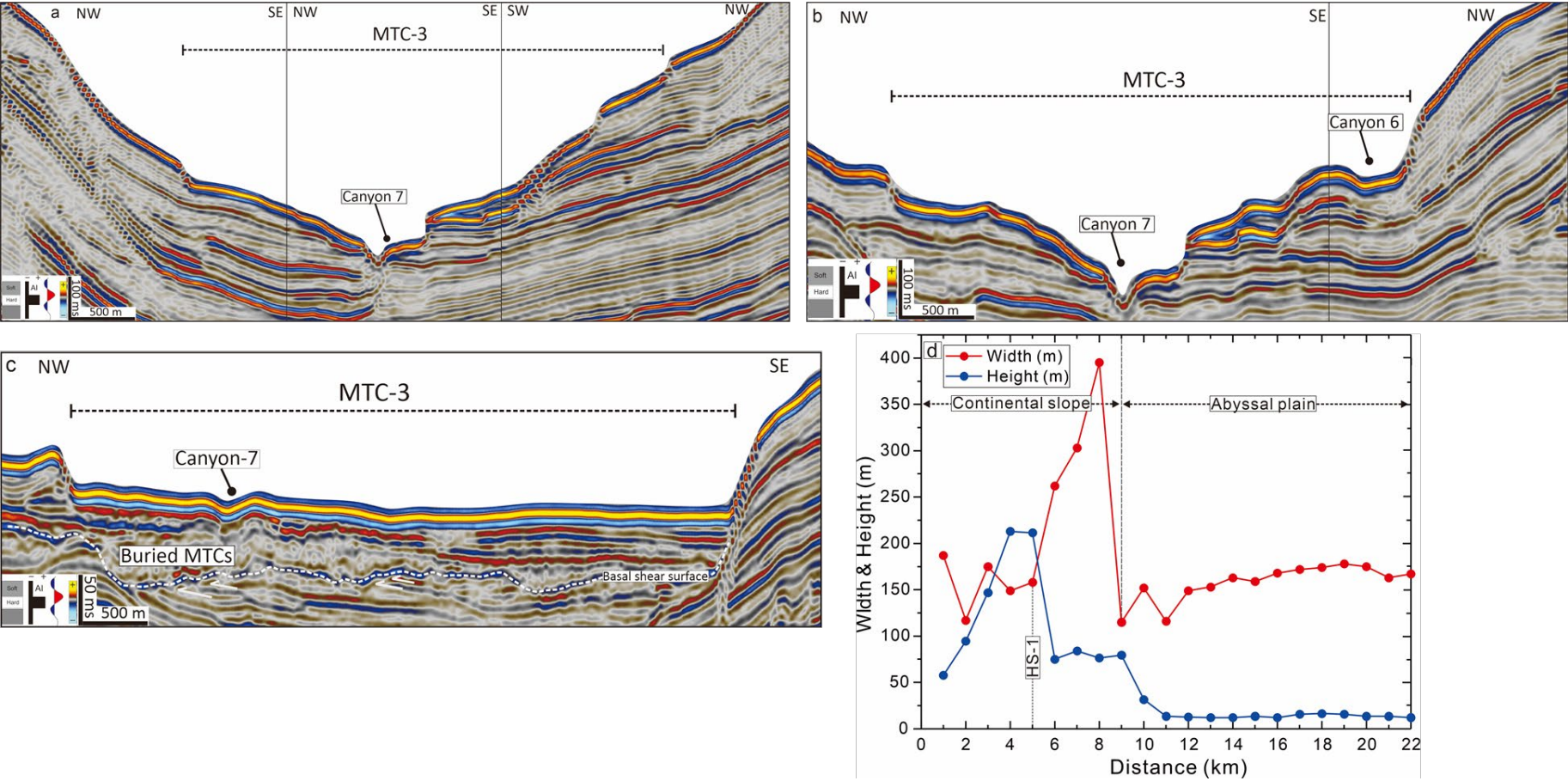


Figure 13

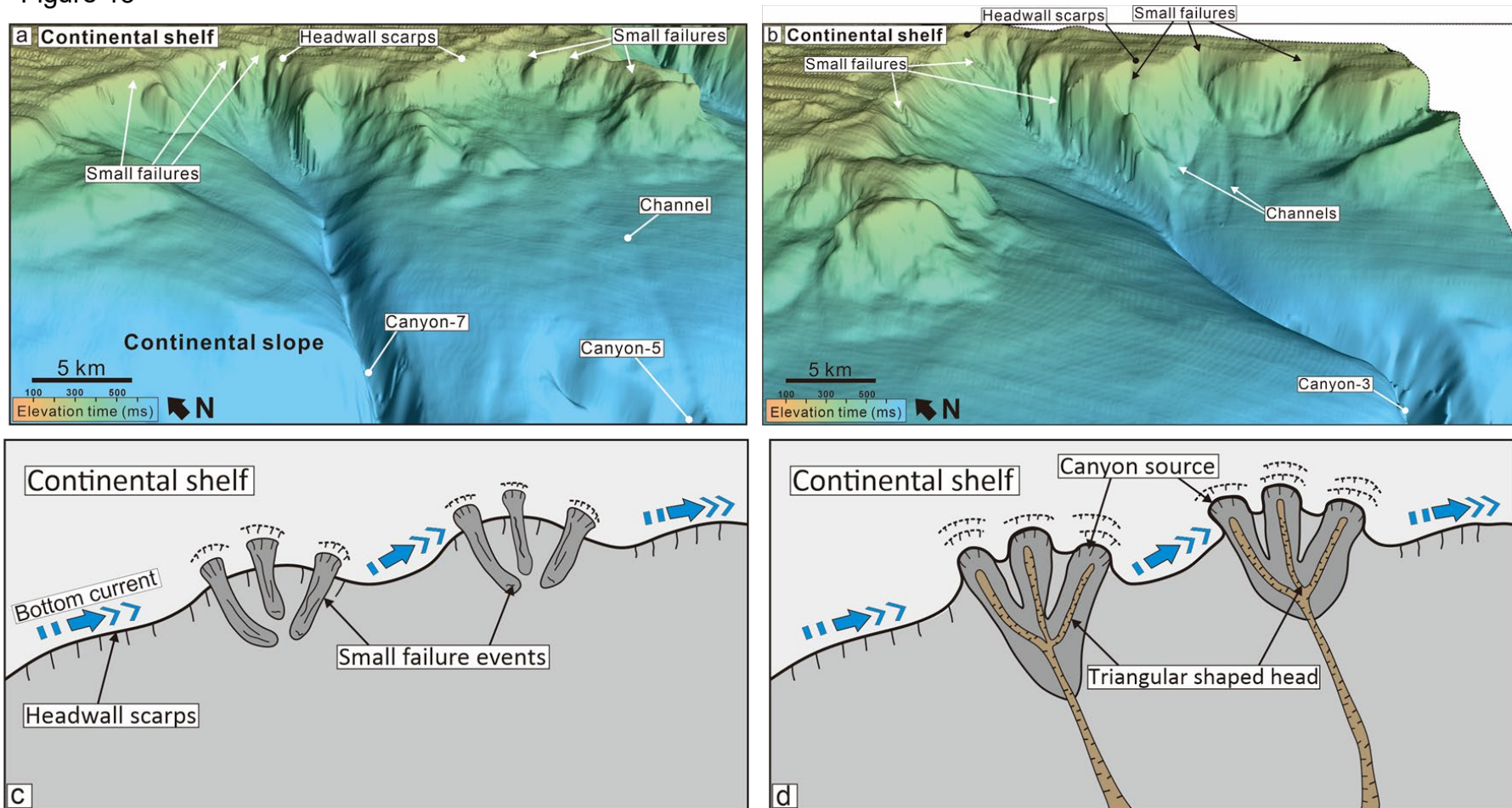
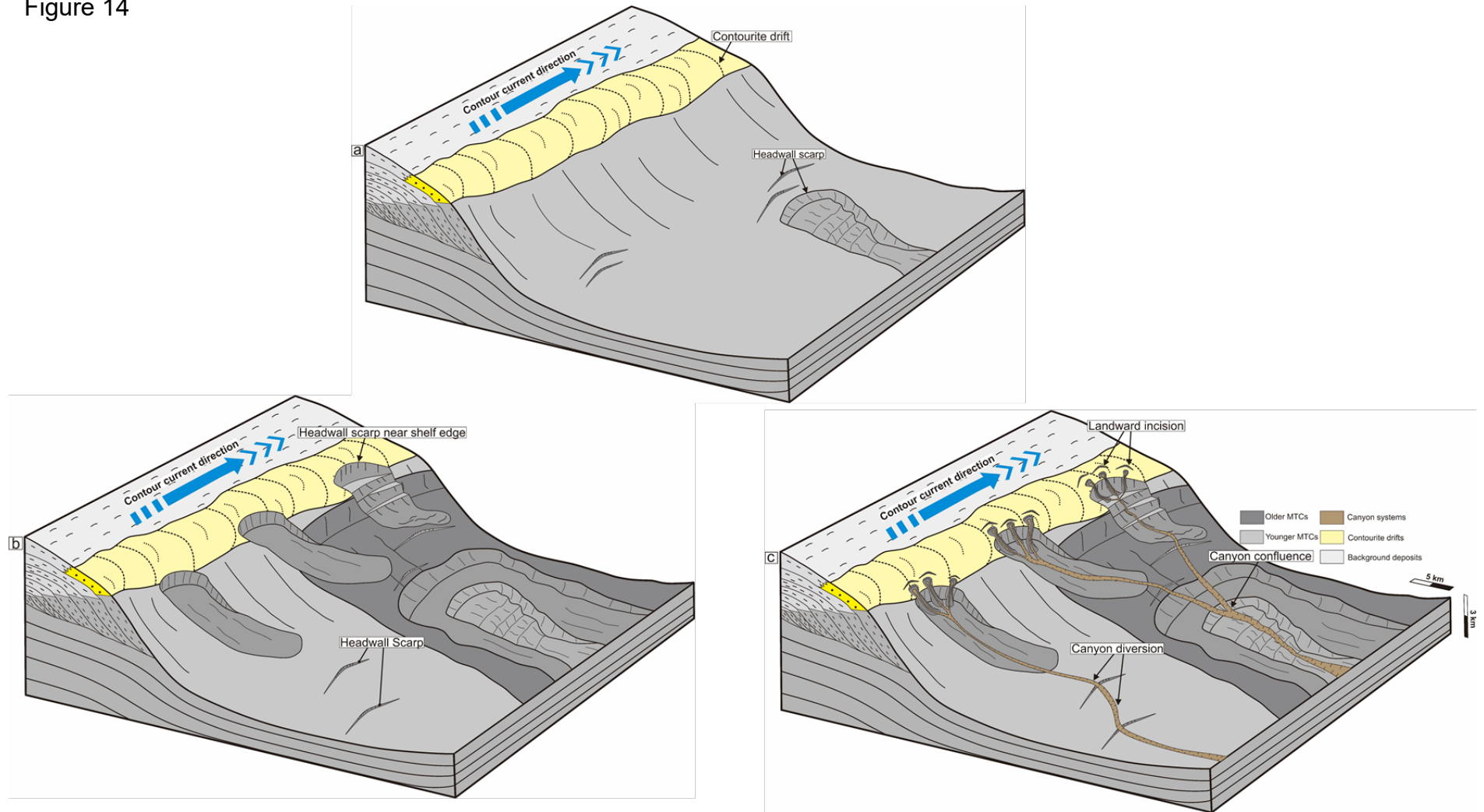


Figure 14



Classification	MTC	Headwall scarps	Canyons	Influences imposed on canyons
Type-1	MTC-1	HS-1 to HS-5	Canyons 1-3	Canyon confluence, widening and deepening
	MTC-2	HS-1 to HS-5	Canyon-5	Canyon transport direction diversion
Type-2	MTC-3	None	Canyons 6-7	No canyon confluence nor diversion

Table 1. Classification of MTCs. Note that MTCs are the abbreviation of mass-transport complexes, and HS equals headwall scarps.